

1 **The contemporary stable isotope hydrology of Lake Suigetsu and surrounding catchment (Japan)**  
2 **and its implications for sediment-derived palaeoclimate records**

3

4 *Rex, Charlie L.<sup>1\*</sup>, Tyler, Jonathan J.<sup>2</sup>, Nagaya, Kazuyoshi<sup>3</sup>, Staff, Richard A.<sup>1</sup>, Leng, Melanie J.<sup>4</sup>,*  
5 *Yamada, Keitaro<sup>5</sup>, Kitaba, Ikuko<sup>5</sup>, Kitagawa, Junko.<sup>3</sup>, Kojima, Hideaki<sup>6</sup>, Nakagawa, Takeshi<sup>5</sup>*

6

7 *\* Corresponding author (c.rex.1@research.gla.ac.uk)*

8 1. Scottish Universities Environmental Research Centre (SUERC), University of Glasgow, Scottish  
9 Enterprise Technology Park, Rankine Avenue, East Kilbride, G75 0QF, United Kingdom

10 2. Department of Earth Sciences, University of Adelaide, Adelaide, South Australia 5000, Australia

11 3. Varve Museum, 122-12-1 Torihama, Wakasa-cho, Mikatakaminaka-gun, Fukui Prefecture, 919-  
12 1331, Japan

13 4. National Environmental Isotope Facility, British Geological Survey, Keyworth, NG12 5GG, UK

14 5. Research Centre for Palaeoclimatology, Ritsumeikan University, 1-1-1 Noji-higashi, Kusatsu,  
15 Shiga Prefecture, 525-8577, Japan

16 6. Wakasa Mikata Jomon Museum, 122-12-1 Torihama, Wakasa-cho, Mikatakaminaka-gun, Fukui  
17 Prefecture, 919-1331, Japan

18

19 **This is a preprint of an article that has yet to be formally accepted for publication. The article has**  
20 **been revised based on one round of reviews from Limnology and Oceanography.**

21 **Abstract**

22 The Lake Suigetsu sediment cores exemplify a high-quality archive of palaeoclimatic change in East  
23 Asia during the past 150 ka. Robust interpretation of stable isotope-based proxy reconstructions  
24 from the Suigetsu cores can be aided by a greater understanding of the factors affecting the isotope  
25 composition of the lake and how it relates to that of precipitation. Here we use extended  
26 contemporary monitoring to establish the factors affecting the stable isotope composition ( $\delta^{18}\text{O}$ ,  
27  $\delta^2\text{H}$  and d-excess) of precipitation, river water and lake water in the catchment surrounding Lake  
28 Suigetsu, central Japan. We show that the composition of precipitation is influenced by the dual  
29 East Asian Monsoon system, producing minima in  $\delta^{18}\text{O}$  and  $\delta^2\text{H}$  and semi-annually varying d-excess  
30 values across the year. These signals are then transferred to the lake system, where they are  
31 combined with secondary local influences on lake water composition: homogenisation with existing  
32 catchment waters, a catchment transit lag, the interaction with saline water from the nearby Sea of  
33 Japan, and evaporative enrichment during summer. Our observations suggest that the palaeo-  
34 isotope composition of Lake Suigetsu was closely related to the behaviour of the East Asian  
35 Monsoon. We highlight lake stratification and proxy seasonality as critical components of signal  
36 interpretation.

37

38 **Keywords**

39 Stable Isotopes; Precipitation Isotopes; Lake Water Isotopes; East Asian Monsoon; Sediment Cores  
40

41 **Introduction**

42 The Five Lakes of Mikata are a collection of tectonic lakes located in Fukui Prefecture, central  
43 Japan, and comprise Lake Mikata, Lake Suigetsu, Lake Suga, Lake Kugushi and Lake Hiruga (Figure  
44 1). To-date, much of the Quaternary research undertaken on the lakes has focussed on Lake Suigetsu,  
45 the central lake of the system, by virtue of its unique underlying sedimentary sequence. This

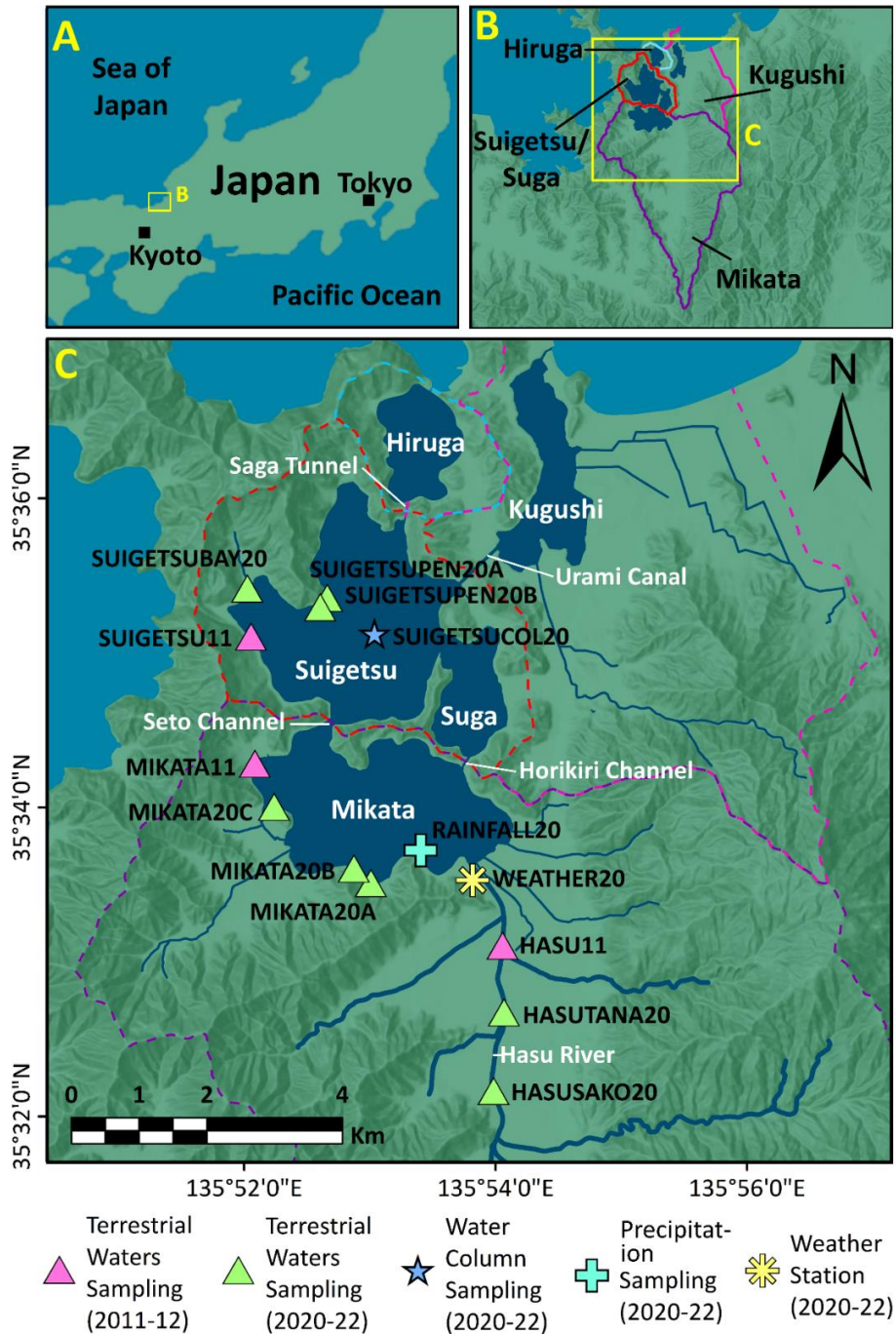
46 sequence is exceptionally well-preserved by a deep water column (34 m) and surrounding hills,  
47 which hinder wind turbation; bottom water anoxia, which prevents bioturbation; and a shallow  
48 connection (the Seto Channel) between Lake Suigetsu and Lake Mikata (upstream of Lake Suigetsu,  
49 Figure 1C), which prevents disturbances by high energy events (Nakagawa *et al.*, 2021). A series of  
50 previous deep coring campaigns have extracted sediment from Lake Suigetsu to generate a high-  
51 quality archive of environmental change (“the Lake Suigetsu sediment cores”) spanning >98 m from  
52 the present day to in excess of 150 ka BP (Nakagawa *et al.*, 2012). A distinctive characteristic of the  
53 Suigetsu cores is that they contain annual laminations (varves) between ~50 and 10 ka BP,  
54 comprising the longest continuously varved record from the Quaternary (Schlolut *et al.*, 2012). The  
55 youngest sediments (up to 50.3 ka BP) have been dated to high precision using radiocarbon dating  
56 of >800 macrofossils (Staff *et al.*, 2011; Bronk Ramsey *et al.*, 2012; Bronk Ramsey *et al.*, 2020), varve  
57 counting using optical microscopy (Schlolut *et al.*, 2012; Schlolut *et al.*, 2018), and analysis of  
58 volcanic tephra deposits with independent ages (e.g., Smith *et al.*, 2011; McLean *et al.*, 2016).  
59 Between 50.3 ka BP and 13.9 ka BP, Lake Suigetsu contributes the only non-reservoir corrected  
60 dataset within the international consensus radiocarbon calibration curve, “IntCal”.

61 It is this excellent archive preservation and world-leading chronological control which makes  
62 multiproxy palaeoenvironmental analyses of the Suigetsu cores an exciting prospect. Indeed, the  
63 location of Lake Suigetsu at a lower latitude than other global benchmark records (e.g., the  
64 Greenland and Antarctic Ice Cores) makes this archive an avenue for establishing a more holistic  
65 global perspective on past climatic change. Additionally, the Japanese archipelago is situated within  
66 the East Asian Monsoon (EAM) regime, a critical, yet complex, component of the global climate  
67 system for which palaeoclimate reconstructions offer a means to greater understanding. Not only  
68 is Japan situated directly beneath the seasonally migrating EAM front, making it sensitive to changes  
69 in the EAM system (Jun-Mei *et al.*, 2013; Nakagawa *et al.*, 2012; Gallagher *et al.*, 2018), but unlike  
70 continental areas, Japan experiences EAM precipitation semi-annually, because both the winter

71 (EAWM) and summer (EASM) prevailing monsoon winds pass over large bodies of water before  
72 reaching the Japanese Islands. Therefore, both seasonal modes have tangible hydrological influence  
73 over precipitation in Japan, and reconstructions from here have the unique potential to determine  
74 the behaviours of both the EAWM and the EASM. In light of this, the Suigetsu cores continue to be  
75 the subject of an ever-growing collection of investigations into climatic change over the last glacial-  
76 interglacial cycle (e.g., Scholaut *et al.*, 2017; Nakagawa *et al.*, 2021), including contributing to the  
77 definition of the Holocene onset as an auxiliary stratotype (Walker *et al.*, 2009). An ongoing avenue  
78 of research is the development of palaeoclimate reconstructions derived from oxygen and hydrogen  
79 isotope compositions of organic matter, pollen grains, biogenic silica and siderite (all of which are  
80 abundant components of the cores), because these offer a means to infer past hydrological change  
81 (including links to EAM behaviour).

82 Robust interpretation of such sedimentary proxies is predicated on a strong understanding  
83 of the controls acting on lake isotope composition ( $\delta_{\text{lake}}$ ), which, in the absence of historical datasets,  
84 can be achieved by extended contemporary monitoring. Of particular interest is the extent to which  
85 variability in the isotope composition of precipitation ( $\delta_{\text{precipitation}}$ , which provides a link to regional-  
86 scale hydrological change) is reflected in the isotope composition of river water ( $\delta_{\text{river}}$ ) and  $\delta_{\text{lake}}$  and,  
87 in turn, lake sedimentary components; however, this depends strongly on catchment and lake  
88 hydrology. Variability in groundwater, river, and in rare cases, marine contributions to the lake  
89 water balance can act to dampen and sometimes conceal the isotope composition of recent  
90 precipitation. In addition, evaporation of lake waters can strongly modify  $\delta_{\text{lake}}$  compared to  
91 inflowing water (Gonfiantini, 1986; Russell and Johnson, 2006; Wassenaar *et al.*, 2011). These  
92 concepts are commonly used in modern hydrology (Gibson *et al.*, 2016); for example, during mass  
93 balance modelling to determine the surface versus groundwater contribution to Lake Ohrid, south-  
94 eastern Europe (Lacey and Jones, 2018) or to consider mass losses due to evaporation, such as for  
95 Lake Edward, East Africa (Russell and Johnson, 2006). Monitoring for an extended period (on the

96 order of years) is required in order to fully understand the evolution of  $\delta_{\text{lake}}$ , particularly in regions  
 97 where the climate is so seasonal. This approach allows for both local influences (such as changing  
 98 inputs and evaporation) to be identified alongside regional scale climatic shifts.



99

100 **Figure 1: Map of the Five Lakes of Mikata catchment.** Yellow outlines show the extent of subsequent panels in  
 101 the sequence. Panel A shows the location of the region in relation to major Japanese cities. Panel B shows the  
 102 catchment area of each lake. Panel C shows the sampling locations for this study, including precipitation sampling,  
 103 river and lake sampling, and sampling of the Lake Suigetsu water column, as well as the location of the weather  
 104 station. Full details of locations shown here are available in Appendix 1. Basemaps: custom World Dark Grey Base  
 105 and World Hillshade from Esri (2022a; 2022b) (scale 1:10,000,000 (panel A), 1:400,000 (panel B), 1:67,946 (panel  
 106 C)).

107 In this study we aimed to better understand the controls acting on the isotope composition  
108 of water within Lake Suigetsu and its surrounding catchment, in order to facilitate interpretation of  
109 isotope-based proxy reconstructions of past climate from the Lake Suigetsu sediment cores. By  
110 monitoring  $\delta_{\text{precipitation}}$ ,  $\delta_{\text{river}}$  and  $\delta_{\text{lake}}$  over a total observation period of two years and ten months  
111 across 2011-2012 and 2020-2022, we assessed the factors affecting the relationships between these  
112 variables. Conceptualising  $\delta_{\text{lake}}$  of Lake Suigetsu is particularly important because whilst the lake and  
113 catchment receive high volumes of precipitation annually, there are other controls which could act  
114 to alter or obscure this precipitation signal; namely, that expected evaporation rates are high due  
115 to a warm summer climate, and in the present day there is some interaction between the lake and  
116 the Sea of Japan. Consequently, resolving the relative influence of  $\delta_{\text{precipitation}}$  (and the propagation  
117 of  $\delta_{\text{precipitation}}$  signals to  $\delta_{\text{lake}}$ ) is crucial to understanding the major controls over long term  $\delta_{\text{lake}}$  within  
118 the context of regional scale hydrological (and thus climatic) change.

119

## 120 **Study Site**

### 121 ***Hydrology***

122 The Five Lakes of Mikata are located adjacent to the towns of Wakasa and Mihama in Fukui  
123 Prefecture, Honshu Island, central Japan. The lakes lie to the west of the active Mikata fault line and  
124 were formed as the western side of the fault subsided over time (Figure 1C; Nakagawa *et al.*, 2012).  
125 Over the last ~400 years, the Five Lakes of Mikata catchment has been anthropogenically influenced  
126 by the construction of channels and tunnels to connect the lakes. In the present day, the lakes form  
127 a route between the freshwater Hasu River and the saline Sea of Japan (Figure 1C). Lake Mikata, the  
128 southernmost lake, is fed by the Hasu River to the south, has an area of ~3.61 km<sup>2</sup> and a maximum  
129 depth of 5.8 m and has the largest discrete catchment area (~50 km<sup>2</sup>; Figure 1B). Lake Mikata is  
130 connected to Lake Suigetsu via the shallow (~2 m deep) Seto Channel, and to the adjacent Lake Suga  
131 via the artificial (<0.5 m deep) Horikiri Channel. Lake Suigetsu, which has an area of ~4.2 km<sup>2</sup> and a

132 maximum depth of 34.0 m, then feeds Lake Hiruga (via the subterranean Saga Tunnel, which was  
133 sealed during the observation period) and Lake Kugushi (via the surficial Urami Canal), which both  
134 flow directly into the Sea of Japan (Shigematsu *et al.*, 1961; Figure 1C). In the past, prior to the  
135 construction of the Horikiri Channel, Saga Tunnel and Urami Canal, Lake Kugushi was a coastal  
136 lagoon (part of Wakasa Bay), and Lake Hiruga was not connected to the sea (except during flooding),  
137 so four of the five lakes were freshwater (Shigematsu *et al.*, 1961; Masuzawa and Kitano, 1982). At  
138 this time, the outflow from Lake Suigetsu was via Lake Suga (effectively a side basin of Lake Suigetsu),  
139 which was connected to Lake Kugushi via a channel (the Kiyama River) through low ground to the  
140 east of the lakes.

141            Principally, water flows in a south-to-north direction through the catchment, driven by the  
142 large quantities of precipitation in the region. However, in the present-day, seawater washes back  
143 into Lake Suga, Lake Suigetsu and Lake Mikata during high tide in autumn (Kondo and Butani, 2007).  
144 As a result, all five lakes now have some degree of marine-derived salinity and observations show  
145 that salinity in the lakes increases during the autumnal high tide and then decreases due to  
146 continued freshwater input via precipitation and surface runoff during winter. Lake Hiruga and Lake  
147 Kugushi are saline, and Lake Mikata is fresh to brackish (0-3 g kg<sup>-1</sup>). Lake Suigetsu and Lake Suga are  
148 both meromictic (permanently stratified), with an upper mixolimnion (aerobic, brackish to saline  
149 water; 2-8 g kg<sup>-1</sup>) separated from a lower monimolimnion (anaerobic, saline water; ~13 g kg<sup>-1</sup>) by a  
150 chemocline at ~8 m depth (Matsuyama, 1974; Kondo *et al.*, 2000; Kondo and Butani 2007). The  
151 mixolimnion exhibits a salinity gradient between the surface (fresh) and the chemocline (saline)  
152 (Matsuyama, 1974; Kondo *et al.*, 2000). Mixing in the mixolimnion occurs once each year, during  
153 the autumn, resulting in an increase in surface water salinity, a raised chemocline and a steepening  
154 of the salinity gradient (Kondo *et al.*, 2000). The chemocline then lowers and a shallower salinity  
155 gradient is re-established during winter. The monimolimnion is a persistent seawater-derived saline  
156 layer, confirmed by geochemical analysis (Shigematsu *et al.*, 1961), and has a limited freshwater

157 influence (Matsuyama, 1973). This layer is replenished annually at the autumnal high tide (Kondo  
158 and Butani, 2007). It is not known whether this autumn seawater incursion drives mixing in the  
159 upper ~8 m of the water column, or if these two processes are merely coincident, although the latter  
160 is suspected. No significant long-term increases in salinity have been observed in the  
161 monimolimnion in the past 70 years; salinity remained approximately 12 to 16 g kg<sup>-1</sup> in the intervals  
162 1951-1966 and 2008-10 (Matsuyama, 1973, Kondo *et al.*, 2014). Complete lake water vertical mixing  
163 events are unusual but have been detected (in 1997; Kondo *et al.*, 2000).

164 The residence time of Lake Suigetsu was calculated to be on the order of ~ 1 year, assuming  
165 a total annual precipitation of ~2.3 m (Japan Meteorological Agency, 2022) across a ~60 km<sup>2</sup>  
166 catchment (~0.14 km<sup>3</sup> precipitation annually) and then applying this to a simple single box model  
167 (surface area of ~4.3 km<sup>2</sup> and ~34 m depth equating to a ~0.15 km<sup>3</sup> volume). However, when  
168 considering the evidence for a stable monimolimnion in Lake Suigetsu with a very long residence  
169 time (Shigematsu *et al.*, 1961), a two-box model is more appropriate, with water effectively flushing  
170 solely through the top ~8 m of the lake (Matsuyama, 1973). In this case, the residence time of the  
171 mixolimnion is on the order of ~3 months.

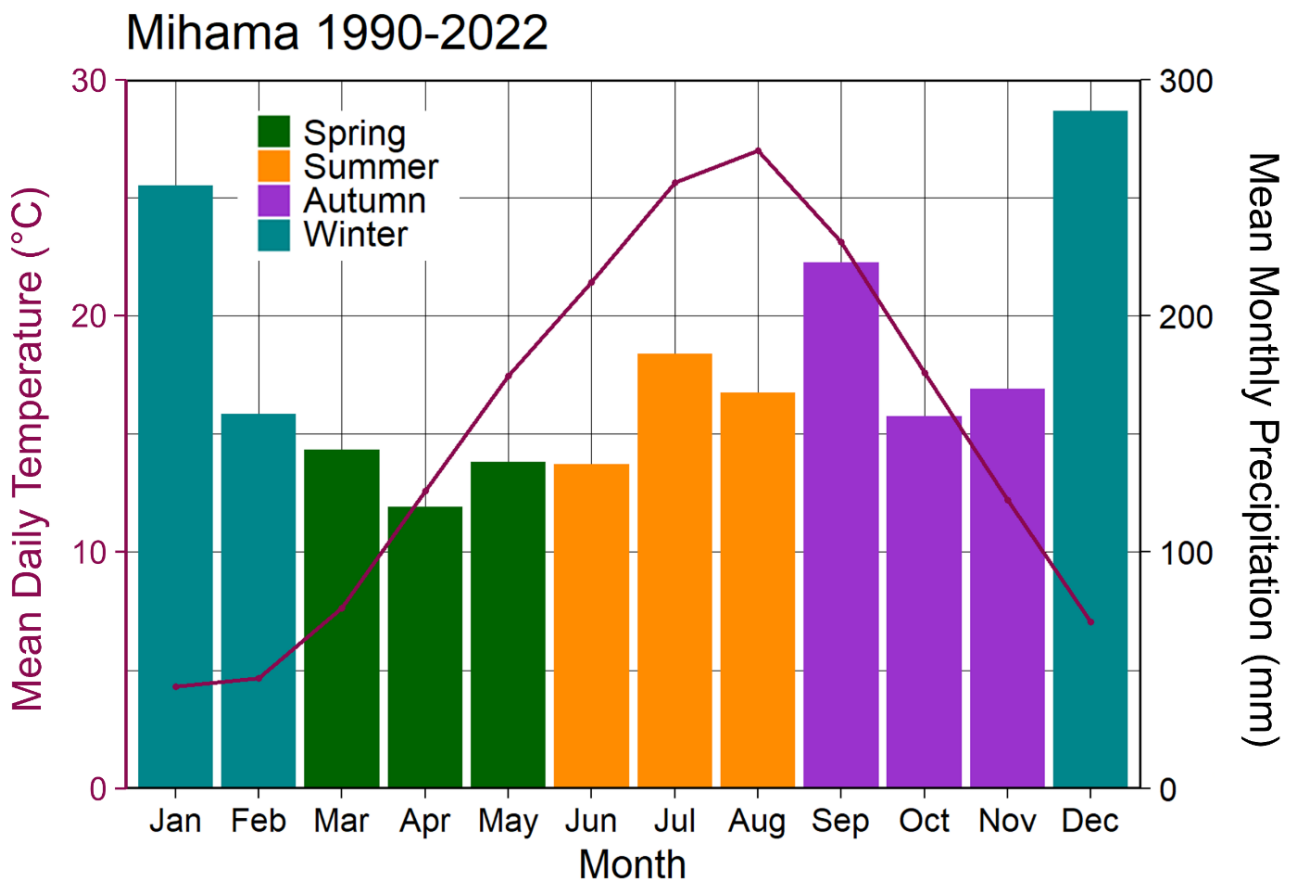
172

### 173 ***Climate***

174 The climate of the Five Lakes of Mikata catchment is temperate with high levels of  
175 precipitation. The temperature profile is typical of Japan, with low temperatures in winter (reaching  
176 a minimum in January with a mean temperature of 4.3 °C) and high in summer (reaching a maximum  
177 in August with a mean temperature of 27.0 °C). The annual distribution of precipitation is more  
178 unusual, because a large proportion of the total annual precipitation falls during winter (Figure 2).  
179 This is unlike much of Japan, where summer is the wettest season. The large quantities of  
180 precipitation received in winter are a result of the catchment being located on the Sea of Japan  
181 coast, where it receives a significant input of EAWM precipitation annually. This EAWM precipitation



182 falls as both rain and snow and is concentrated in December and January. Spring (March to May) is  
 183 the driest season of the year, which precedes a second rainy period in early summer which  
 184 accompanies the EASM. The EASM rainy season is known as the *Tsuyu* or *Baiu*, which occurs at Lake  
 185 Suigetsu around late June into July, immediately prior to the period of maximum temperature. This  
 186 is followed by typhoon season from August to September, during which a series of low-pressure  
 187 systems pass over Japan from the Pacific Ocean to the south, resulting in a third annual period of  
 188 rain. Winter (EAWM) and summer (EASM) precipitation are the most significant extended  
 189 (persistent) freshwater inputs to the catchment; typhoon season precipitation comprises a series of  
 190 intense isolated precipitation events.



191  
 192 **Figure 2: Climate at the Five Lakes of Mikata.** Monthly variations in mean daily temperature (pink curve) and  
 193 mean total monthly precipitation (bars) at Mihama, adjacent to Lake Kugushi (35°36'00"N 135°55'00"E). Data from  
 194 the Japan Meteorological Agency, 1<sup>st</sup> January 1990 to 28<sup>th</sup> February 2022.  
 195

196 **Materials and Methods**

197 ***Sampling Methods***

198 Samples of lake and river waters (n = 463) were taken from the Hasu River, Lake Mikata and  
199 Lake Suigetsu (Figure 1C) on a weekly basis between 1<sup>st</sup> March 2011 and 3<sup>rd</sup> January 2012, and again  
200 between 15<sup>th</sup> July 2020 and 29<sup>th</sup> July 2022. Water was collected by submerging a collection vessel in  
201 the top ~50 cm of water before subsampling using a vial leaving no or minimal head space. Precise  
202 sampling locations were altered between the 2011/12 and 2020/22 sampling intervals, and during  
203 periods of inaccessibility (e.g., due to bridge repairs, snowfall, lake freezing and flooding; Appendix  
204 1). The slight changes in sampling location are unlikely to affect the isotope composition recorded,  
205 being within the same water depth range and situated away from lake inputs. If visible algae were  
206 present in the water, the samples were filtered using a 50 µm polyethylene terephthalate (PET)  
207 mesh filter. Surface water data from the 2011-2012 observation period do not have the  
208 accompanying (precipitation and water column) data described below because this was an  
209 extended pilot study focussed on the river and lake waters; however, we have nevertheless included  
210 these 2011-2012 data in our analysis because there are subtle differences in these data that  
211 contribute to a more comprehensive view of isotope variations in the catchment.

212 Precipitation samples (n = 120) were captured between 13<sup>th</sup> July 2020 and 29<sup>th</sup> July 2022  
213 using a purpose built (3D printed) funnel and glass bottle holder in Wakasa (at the location indicated  
214 in Figure 1C). Silicone oil was added to the collection bottle to prevent evaporation. Water  
215 subsamples were taken from the bottle using a Teflon pipette. Subsamples were taken on an event  
216 basis; every day during periods of frequent precipitation, but less often during periods of reduced  
217 precipitation. The water was allowed to overflow the sample vial in order to remove the floating  
218 silicone oil. Fresh snowfall samples were collected from pristine areas of snow after deposition and  
219 melted with silicone oil in a lidded container before being transferred to the collection vial. An  
220 automated Netatmo weather station (location also shown in Figure 1C) was deployed to provide

221 temperature, humidity, precipitation amount and wind data to accompany the isotope data.  
222 Backwards air parcel trajectory analysis was performed for four precipitation events (representative  
223 of each season) using the NOAA Air Resources Laboratory HYSPLIT model (Stein *et al.*, 2015, Rolph  
224 *et al.*, 2017). The selected events ended on 27<sup>th</sup> December 2020, 16<sup>th</sup> September 2021, 2<sup>nd</sup> May 2022  
225 and 7<sup>th</sup> July 2022, respectively. Back trajectories were generated for air parcels arriving at the  
226 catchment every 12 hours at 1500 m.a.s.l. across a 72-hour window prior to the end of each event.

227 Water column profiling was conducted ~quarterly on 22<sup>nd</sup> December 2020, 8<sup>th</sup> April 2021,  
228 5<sup>th</sup> August 2021, 17<sup>th</sup> November 2021, 23<sup>rd</sup> April 2022 and 21<sup>st</sup> July 2022 at the approximate centre  
229 of Lake Suigetsu (Figure 1C). Samples were taken every 2 m between the surface and 10 m depth,  
230 every 5 m between 10 m and 30 m depth, and then every 2 m between 30 m and 34 m (n = 70). A  
231 sealable van Dorn water sampler was used to prevent mixing of the sample with water at different  
232 depths during transit to the surface. A Hydrolab DS5 water quality meter was also used to measure  
233 temperature and salinity profiles on each sampling date; higher resolution geochemical data were  
234 collected for the December 2020, April 2021, November 2021, April 2022 and July 2022 dates. The  
235 low-resolution data collected for the August 2021 date (using a TOA-DKK WQC-24 meter) are also  
236 shown in the Results and Interpretation section below.

237

### 238 **Analytical Methods**

239 Oxygen isotope ( $\delta^{18}\text{O}$ ) measurements were made using an Isoprime 100 mass spectrometer  
240 with an Aquaprep dual-inlet system using the  $\text{CO}_2$  equilibration method. Subsamples (totalling 200  
241  $\mu\text{l}$ ) were placed in a heated sample tray at 40 °C before the air was evacuated and each exetainer  
242 was flushed with  $\text{CO}_2$ . The samples were then left to equilibrate for between 12 (first sample) and  
243 37 (last sample) hours. Any remaining water vapour was then removed on a sample-by-sample basis  
244 using a cryogenic water trap, before each sample was expanded into the dual inlet isotope ratio  
245 mass spectrometer (IRMS) for analysis. The samples were measured in alternate pulses alongside a

246 reference CO<sub>2</sub> gas, and the integrated values of the sample were compared to the reference gas  
247 values to determine <sup>18</sup>O/<sup>16</sup>O. Two internal laboratory standards (CA-HI and CA-LO) were analysed in  
248 each run. The value of these standards has been determined accurately by comparison with  
249 international calibration and reference materials (VSMOW2, SLAP2 and GISP). This facilitated the  
250 calculation of the <sup>18</sup>O/<sup>16</sup>O ratio of each sample versus VSMOW2, and subsequent expression of the  
251 oxygen isotope ratio in delta (δ) units (δ<sup>18</sup>O) in parts per mille (‰). The typical standard deviation is  
252 <0.05 ‰.

253 Hydrogen isotope (δ<sup>2</sup>H) measurements were made in duplicate using a continuous flow, high  
254 temperature conversion elemental analyser - IRMS (TC-EA-IRMS) (EuroPyrOH-Isoprime) with liquid  
255 autosampler. Subsamples (0.5 μl) were injected into a heated septa-sealed port at 160 °C and  
256 converted to water vapour. The vapourised sample was then flushed through a chromium-packed  
257 reactor at 980 °C by the helium carrier gas, which reduced the water to hydrogen gas. A reference  
258 hydrogen gas pulse was introduced to the IRMS prior to the gas pulse from each sample. The sample  
259 peaks were then integrated and corrected for the H<sub>3</sub><sup>+</sup> contribution before comparison to the  
260 reference gas to yield <sup>2</sup>H/<sup>1</sup>H. Each sample was measured five times. As with the oxygen isotope  
261 measurements, the samples were then compared to measurements of CA-HI and CA-LO to calculate  
262 the <sup>2</sup>H/<sup>1</sup>H ratio of each sample versus VSMOW2, and expression of the hydrogen isotope ratio in  
263 delta units as for the oxygen isotopes. The typical standard deviation is <0.5 ‰.

264 The aforementioned δ<sup>18</sup>O and δ<sup>2</sup>H measurements were then used to calculate d-excess  
265 (Equation 1), a second-order parameter which can be considered as a measure of deviation from  
266 the Global Meteoric Water Line (GMWL, which has a gradient of 8). This occurs when there is a  
267 greater amount of <sup>2</sup>H relative to <sup>18</sup>O, caused by diffusive fractionation during evaporation of water  
268 molecules (Bershaw, 2018).

269

$$270 \quad \text{d-excess} = \delta^2\text{H} - (8 * \delta^{18}\text{O}) \quad \text{(Equation 1)}$$

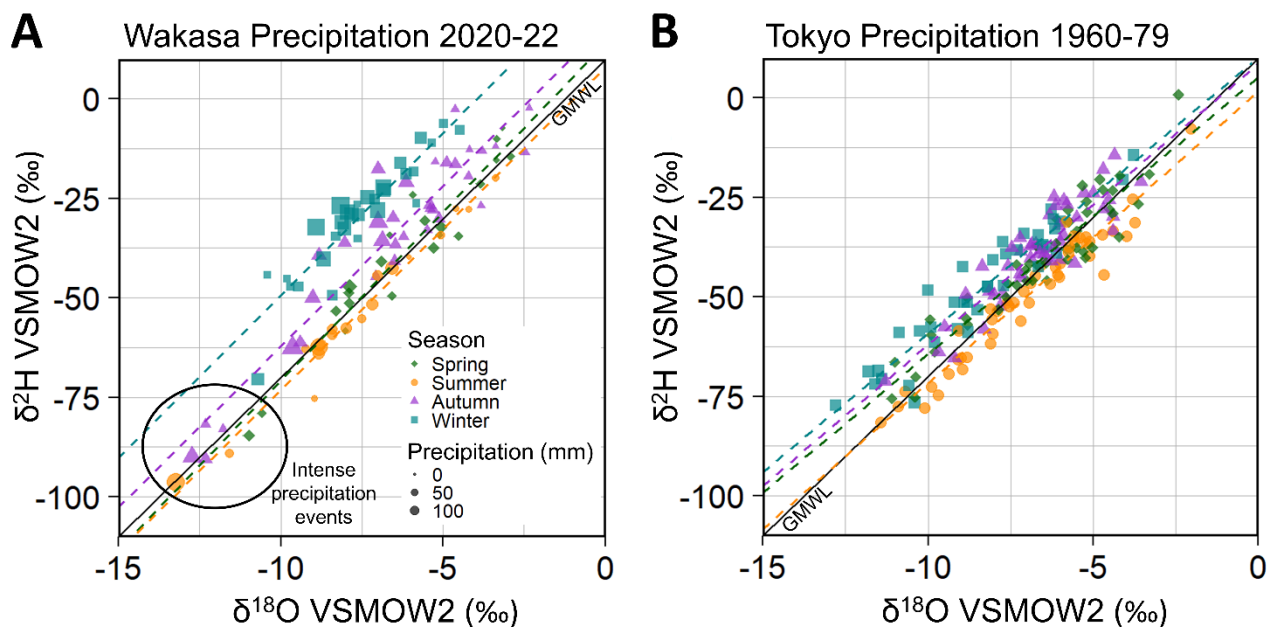
271 **Results and Interpretation**

272 ***Precipitation  $\delta^{18}\text{O}$  and  $\delta^2\text{H}$***

273 Values of  $\delta^{18}\text{O}$  for the precipitation at Wakasa (July 2020 to July 2022) ranged from -13.2 ‰  
274 to -2.4 ‰, with a mean value of -7.0 ‰ and standard deviation of 1.6 ‰ (Figure 3A).  $\delta^2\text{H}$  values  
275 ranged from -96.4 ‰ to 2.3 ‰, with a mean of -39.1 ‰ and standard deviation of 11.9 ‰. Figure  
276 3A shows only small seasonal differences in  $\delta^{18}\text{O}$  and  $\delta^2\text{H}$  because there was considerable intra-  
277 seasonal variability and overlap. Throughout the study period,  $\delta^{18}\text{O}$  and  $\delta^2\text{H}$  were associated with  
278 rapid high amplitude fluctuations with time (Figure 4); however, winter and summer minima were  
279 observed when the data were considered on a monthly basis; likely due to greater quantities of  
280 precipitation (Figure 2) during these seasons (discussed further below). This trend was clearest in  
281 the  $\delta^{18}\text{O}$  values, but a summer minimum was also observed in the  $\delta^2\text{H}$  values (Figure 4); the winter  
282 minimum likely obscured by high d-excess values (described below). Back trajectory analysis of four  
283 precipitation events from across our sampling period indicates that air parcels arriving at the  
284 catchment predominately originated over Continental Asia during the winter, in the oceanic domain  
285 (Pacific Ocean, Philippine Sea and East China Sea) during summer, and a mixture of the two during  
286 the spring and autumn (Figure 5).

287 These trajectories, which ultimately reflect the operation of the EAM as dual EAWM and  
288 EASM modes, highlight the influence of the EAM on the climate of Japan, and can explain the lack  
289 of distinctive seasonal precipitation  $\delta^{18}\text{O}$  and  $\delta^2\text{H}$  trends at Wakasa. EAWM and EASM precipitation  
290 over Japan generally have very similar compositions (Taniguchi *et al.*, 2000; Uemura *et al.*, 2012) in  
291 direct contrast to Continental Asia, where EAWM and EASM precipitation exhibit distinct  
292 compositions due to continental ( $\delta^{18}\text{O}_{\text{precipitation}} \sim -4$  ‰) versus oceanic sources ( $\delta^{18}\text{O}_{\text{precipitation}} \sim -$   
293  $10$  ‰), and hence vary seasonally (Araguas-Araguas *et al.*, 1998). EAWM air masses originate in  
294 central Asia and Siberia and are predominately cold and dry, and hence whilst distillation and  
295 moisture recycling earlier in the trajectory is possible, the isotope signal of EAWM precipitation over

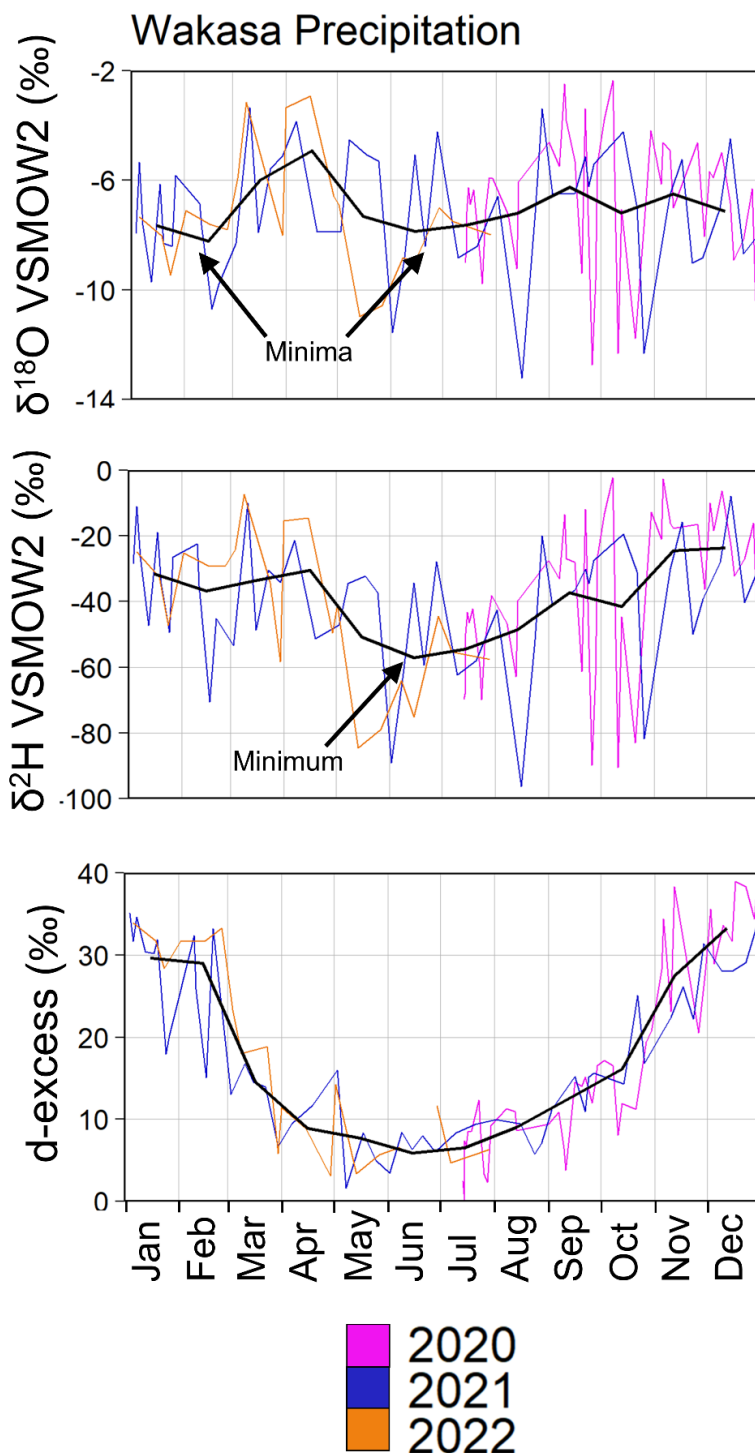
296 Japan is dominated by the interaction of this air mass with the Sea of Japan. The evaporation from  
 297 the Sea of Japan in winter has a light isotope signal ( $\delta^{18}\text{O} \sim -8 \text{‰}$ ; Uemura *et al.*, 2012) and the  
 298 transport distance is short (on the order of  $<1000 \text{ km}$ ), so this signal is retained in winter  
 299 precipitation  $\delta^{18}\text{O}$  and  $\delta^2\text{H}$  (i.e., little further depletion of the heavier isotopes occurs during  
 300 transport). Conversely, EASM air masses originate over the Pacific Ocean and track towards the  
 301 Japanese archipelago via the Philippine Sea and East China Sea (the trajectory ultimately determined  
 302 by the positioning of the Western Pacific Subtropical High (Xu *et al.*, 2020; Figure 5). Evaporation  
 303 from this oceanic domain has a range of isotope compositions (from  $\delta^{18}\text{O} \sim -4 \text{‰}$  in the Western  
 304 Pacific Warm Pool to  $\delta^{18}\text{O} \sim -8 \text{‰}$  in the East China Sea; Uemura *et al.*, 2012); however, the distance  
 305 from the sources with a heavier isotope signal to Japan is greater, such that overall depletion of the  
 306 heavier isotopes during transport acts to minimise differences between proximal and distal sources.  
 307 As such, EASM  $\delta^{18}\text{O}$  and  $\delta^2\text{H}$  is low, as with the EAWM.



|        | Wakasa   |           | Tokyo    |           |
|--------|----------|-----------|----------|-----------|
|        | Gradient | Intercept | Gradient | Intercept |
| Spring | 8.5      | 13.9      | 7.0      | 5.1       |
| Summer | 7.8      | 8.1       | 7.3      | 1.6       |
| Autumn | 8.1      | 18.5      | 7.1      | 8.5       |
| Winter | 8.2      | 32.2      | 7.2      | 12.7      |

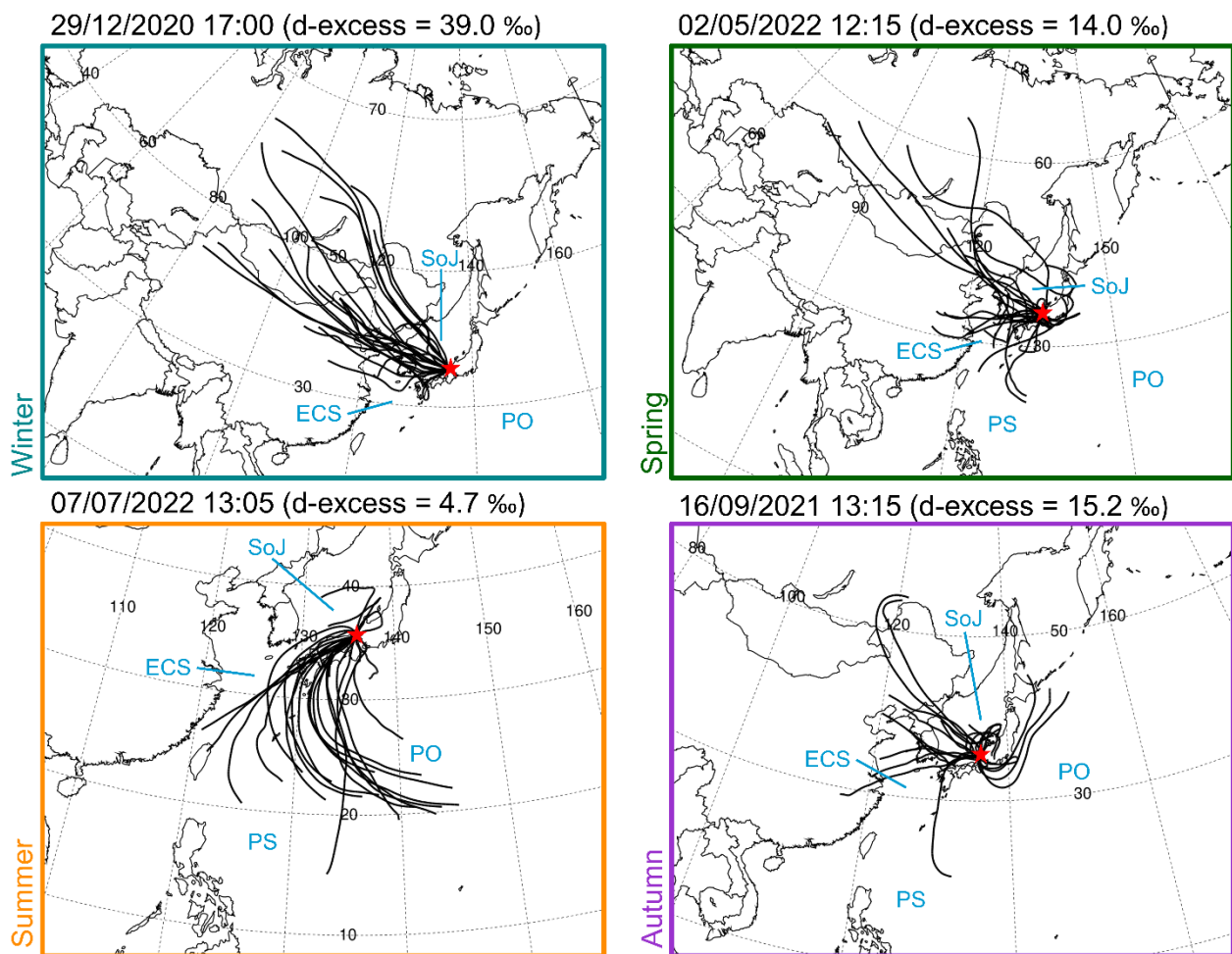
308

309 **Figure 3: Precipitation  $\delta^{18}\text{O}$  and  $\delta^2\text{H}$  at Wakasa and Tokyo.** A comparison of isotopes in precipitation at (A)  
 310 Wakasa 2020-22 (event basis, Sea of Japan Coast) and (B) Tokyo 1960-79 (monthly averages, Pacific Ocean Coast).  
 311 Linear regression local meteoric water lines for each season are shown and numerically described in the table.  
 312 Black diagonal lines represent the Global Meteoric Water Line (GMWL). The points plotted for the composition of  
 313 Wakasa are scaled by quantity of precipitation (as calculated from the Wakasa weather station; WEATHER20 in  
 314 Figure 1). Seasons are defined as: Spring (Mar-May), Summer (Jun-Aug), Autumn (Sep-Nov), Winter (Dec-Feb). d-  
 315 excess is higher for points above the GMWL.  
 316



317

318 **Figure 4: Variations in  $\delta_{\text{precipitation}}$  with time.**  $\delta^{18}\text{O}$ ,  $\delta^2\text{H}$  and d-excess values from precipitation at Wakasa from  
 319 across the study period (colour lines). Black lines represent monthly averages of each dataset.



320

321 **Figure 5: HYSPLIT back trajectory model results.** HYSPLIT back trajectory model results for four rainfall events  
 322 across the 2020-22 rainfall study period. Events were selected to cover a range of d-excess values which are typical  
 323 of each of the four seasons. Dates and times indicate the end of each sampling interval. Red stars indicate the  
 324 position of the catchment; backtrack analysis was performed to the exact position of the precipitation sampler  
 325 (RAINFALL20 in Figure 1.1). Surrounding seas and oceans are labelled as follows: SoJ = Sea of Japan, ECS = East  
 326 China Sea, PS = Philippine Sea, PO = Pacific Ocean.  
 327

328 This similarity in the composition of precipitation from each end member trajectory likely  
 329 results in the limited seasonality that we observed at Wakasa. The air parcel trajectories during  
 330 spring and autumn exhibited mixed behaviour, and we suggest that this lack of strong prevailing  
 331 wind direction and a mixture of vapour sources during these intermediate seasons produced  
 332 precipitation with a similar composition to the EAM months, although we suspect that the spring  
 333 and autumn values were slightly higher due to relatively reduced quantities of precipitation during  
 334 these seasons (discussed further below). Intra-seasonal variability was likely due to subtle  
 335 differences in the airmass trajectories associated with each precipitation event.



336 Very low  $\delta^{18}\text{O}$  and  $\delta^2\text{H}$  values (in the  $\delta^{18}\text{O}$  range of -13.2 ‰ to -11.0 ‰) were uncommon at  
337 Wakasa; however, a minor cluster of precipitation events was nevertheless associated with such  
338 values (Figure 3A). The majority of these datapoints represent precipitation from August to October  
339 (Figure 4) and include rains from Tropical Storm Dolphin (2020). Given the seasonality of such events,  
340 a simple explanation could be that this precipitation was derived from tropical storms (typhoons),  
341 which are associated with  $\delta^{18}\text{O}$  values up to 6 ‰ lower than other summer precipitation events,  
342 driven by strong fractionation processes in heavy cyclonic precipitation (Lawrence and Gedzelman,  
343 1996; Fudeyasu *et al.*, 2008; Li *et al.*, 2010; Jackisch *et al.*, 2022). However, it is worth noting that  
344 precipitation from earlier months of the year also occasionally exhibited these values, and other  
345 typhoon events did not. Instead, we posit that these compositions were associated more generally  
346 with intense precipitation events. Whilst they do not universally correspond to periods with large  
347 quantities of precipitation, this does not preclude a relationship with intense precipitation events  
348 because our analysis considered only the total amount of precipitation which fell in the collection  
349 period, not the intensity. Not all typhoon events result in intense precipitation at Wakasa due to its  
350 location, and many typhoons are associated with high wind speeds alone; hence, some were not  
351 associated with very low isotope values during the study period.

### 352 ***Precipitation d-excess***

353 In contrast to the  $\delta^{18}\text{O}$  and  $\delta^2\text{H}$  datasets, we observed very clear high-amplitude seasonal  
354 patterns in precipitation d-excess, which exhibited an average value of 17.1 ‰ and range of 35.6 ‰  
355 across the entire dataset (Figure 3A). The values for summer precipitation fell broadly along the  
356 GMWL, whereas winter precipitation consistently expressed higher d-excess values, offset yet  
357 parallel to the GMWL (Figure 3A). The autumn and spring d-excess values exhibited intermediate  
358 values with some overlap with summer and winter, particularly so for the autumn. Regression lines  
359 between  $\delta^{18}\text{O}$  and  $\delta^2\text{H}$  applied to each season had similar gradients ( $\sim 8$ ), with minor differences due  
360 to the relatively limited amount of data across a narrow range. The difference in intercept between

361 the summer and winter regression lines was 24.1 ‰ (equating to a difference in seasonally averaged  
362 d-excess of 23.5 ‰).

363 Collective observations of d-excess at sites across Japan suggest that this variable shows this  
364 distinct pattern regardless of location (Uemura *et al.*, 2012; Hasegawa *et al.*, 2014; Ichiyanagi and  
365 Tanoue, 2016). High values of d-excess in winter precipitation and low values in summer  
366 precipitation can be attributed to contrasting relative humidity values in the precipitation source  
367 regions, which overprints the d-excess of the source water itself (Xia *et al.*, 2018; Uemura *et al.*,  
368 2012). Due to cooler sea surface temperatures (and thus low relative humidity) over the Sea of Japan  
369 during the winter, we suggest that winter (EAWM) precipitation exhibits higher d-excess values  
370 relative to summer (EASM) precipitation, which originates from the oceanic domain during the  
371 summer where relative humidity is high (Araguas-Araguas *et al.*, 1998; Kurita *et al.*, 2015). Relative  
372 humidity can affect d-excess via multiple mechanisms, but in the low latitudes the dominant control  
373 is the amount of raindrop re-evaporation, and in the mid latitudes oceanic evaporation conditions  
374 show greater significance (Xia *et al.*, 2022). The gradual transition of influence between these  
375 contrasting extremes suggests that there were no abrupt shifts or interfaces between systems at  
376 play in this region during spring or autumn and instead, hydrologically, Japan transitioned gradually  
377 between the influence of the EAWM and EASM operational modes; supported by the back trajectory  
378 analysis (Figure 5).

### 379 ***Quantity-weighted composition***

380 The largest precipitation events during our study interval occurred during winter and, to a  
381 lesser extent, during the late summer and early autumn (Figure 3A), which is in line with the long-  
382 term climate data from nearby Mihama (Figure 2). The largest winter events exhibited higher d-  
383 excess values, whilst the largest late summer/early autumn events showed low  $\delta^{18}\text{O}$  and  $\delta^2\text{H}$  values  
384 (as discussed above). This has important implications for the introduction of precipitation to the  
385 catchment; most notably, this indicates that the largest contribution to the catchment on an annual

386 basis is that of a mid-range isotope composition (with high d-excess), with a secondary component  
387 having low  $\delta^{18}\text{O}$  and  $\delta^2\text{H}$  values (with low d-excess). When weighted by precipitation amount, the  
388 annual mean  $\delta^{18}\text{O}$  was  $-7.4\text{‰}$ , the annual mean  $\delta^2\text{H}$  was  $-39.7\text{‰}$  and the annual mean d-excess  
389 was  $19.8\text{‰}$ , which lies between the winter and autumn regression lines. A caveat to this is that the  
390 values used to calculate precipitation amount for this analysis were measured by the Netatmo  
391 weather station, which did not contain a heating element, so the quantity of precipitation may be  
392 underestimated for snowfall events and hence the precipitation-weighted annual mean  $\delta^{18}\text{O}$  and  
393  $\delta^2\text{H}$  values may lie closer to the winter average. Snowfall events are likely to be amongst the smallest  
394 winter precipitation events in Figure 3A, however, the relatively tight grouping of winter values  
395 suggests that the difference between snowfall and rainfall isotope values was not particularly  
396 marked across the observation period.

#### 397 ***Temperature and amount effects***

398 Additional analysis (least-squares linear regression) was performed using the precipitation  
399  $\delta^{18}\text{O}$  and  $\delta^2\text{H}$  values to provide an indication of the influence of a “temperature effect” or  
400 precipitation “amount effect”. The isotope data were compared to the average temperature and  
401 the total precipitation amount (square root transformed) during each collection period, as  
402 measured by the Netatmo weather station (position indicated in Figure 1C). These analyses were  
403 conducted using monthly average  $\delta^{18}\text{O}$  and  $\delta^2\text{H}$  values (to reduce the influence of noise) and then  
404 repeated using datapoints from each season in isolation, and the full results are presented in  
405 Appendix 2. All of the calculated  $R^2$  values were low (0.00 – 0.34), suggesting that neither  
406 temperature nor precipitation amount explained a large proportion of variability in precipitation  
407  $\delta^{18}\text{O}$  or  $\delta^2\text{H}$ . Our findings are in line with other studies, which have suggested that local  
408 meteorological parameters are not as prominent as source region and transport effects on  
409 precipitation isotopes in Japan (e.g., Hasegawa *et al.*, 2013; Ichiyangi *et al.*, 2016); however, others  
410 have found that they can retain moderate influence on a local scale (Ichiyangi and Tanoue, 2016).

411 Our  $R^2$  values are similar to those presented by Ichiyanagi and Tanoue (2016), who found that the  
412  $\delta^{18}\text{O}$  of precipitation in Fukui City, ~60 km from Lake Suigetsu, showed weak to no correlation with  
413 either temperature ( $R^2 = 0.02$ ) or precipitation amount ( $R^2 = 0.14$ ).

414         Analysing the data by season allows for changes in more dominant influences (e.g., opposing  
415 precipitation sources) to be minimised, and thus any obscured temperature and amount effects to  
416 be more easily identified. Indeed, this method reveals a stronger relationship between precipitation  
417 amount and isotope composition in spring, summer and autumn (but no relationship to  
418 temperature during those seasons). This suggests that there was a small amount effect acting on  
419 isotopes in precipitation at Wakasa, but no observable temperature effect on event-based  
420 timescales. Conversely, winter precipitation isotopes were very weakly correlated with temperature  
421 ( $R^2(\delta^{18}\text{O}) = 0.18$ ) and not correlated with precipitation amount ( $R^2(\delta^{18}\text{O}) = 0.00$ ). However, as  
422 previously mentioned, the Netatmo weather station did not contain a heating element and hence  
423 snowfall amount was underestimated. Hence, we posit that there may have been a small amount  
424 effect influencing precipitation isotopes during winter, in line with other seasons, but this was not  
425 accounted for by our methods. This analysis suggests that the amount effect was a second-order  
426 control on isotopes in precipitation at Wakasa but was obscured by seasonality. Indeed, our dataset  
427 provides further qualitative evidence for such an amount effect because we observed minima in  
428 precipitation  $\delta^{18}\text{O}$  and  $\delta^2\text{H}$  coinciding with the periods of greatest precipitation amount (excluding  
429 the winter  $\delta^2\text{H}$  minimum, observed by high d-excess values) and attributed very low  $\delta^{18}\text{O}$  and  $\delta^2\text{H}$   
430 values to intense precipitation events. It might be expected that a clearer relationship would be  
431 observed between precipitation  $\delta^{18}\text{O}$  and  $\delta^2\text{H}$  and the integrated amount of precipitation from  
432 across the entire transport pathway (as proposed by Uemura *et al.* (2012)). A lack of any  
433 temperature effect was not unexpected, because it has been posited that temperature effects  
434 merely explain spatial, not temporal, differences in precipitation isotope composition (Ichiyanagi *et*  
435 *al.*, 2016).

## 436 ***Comparison to Tokyo***

437           The isotope composition of precipitation at Wakasa and the nearest GNIP station at Tokyo  
438 (350 km to the east) was very similar, albeit with some key disparities (Figure 3B). The same seasonal  
439 patterns in d-excess were observed at both locations, with the summer and winter values acting as  
440 end members, and intermediate spring and autumn values. However, compared to Wakasa, the  
441 seasonal difference at Tokyo was much less distinct, and the difference between the summer and  
442 winter regression line intercept was only 11.1 ‰ (reflecting a difference in seasonally averaged d-  
443 excess of 13.0 ‰). This is most likely due to a smaller relative influence of EAWM precipitation  
444 (which is associated with the highest d-excess values); Wakasa is located on the Sea of Japan coast,  
445 where there is a strong EAWM (and thus Sea of Japan) influence, and Tokyo is located on the Pacific  
446 coast, where these influences are significantly weaker. Instead, winter precipitation at Tokyo  
447 generally falls in short duration events that result from recycled local water. The local meteoric  
448 water line gradients were also shallower and more consistent at Tokyo across the seasons; however,  
449 this is likely to be the result of a larger dataset from Tokyo which captured values over a longer  
450 timescale. It is important to note that these datasets do not have the same resolution or cover the  
451 same period (the Wakasa precipitation dataset is on an event-basis over 2020-22, and the Tokyo  
452 precipitation dataset is monthly from 1961-79); however, the same trends are observed when the  
453 Wakasa precipitation data is considered at a monthly resolution, and also in comparison to event-  
454 based data from Tokyo in 2013 (Appendix 3; Ichiyanagi and Tanoue, 2016). Hence, the comparisons  
455 made here are reasonable.

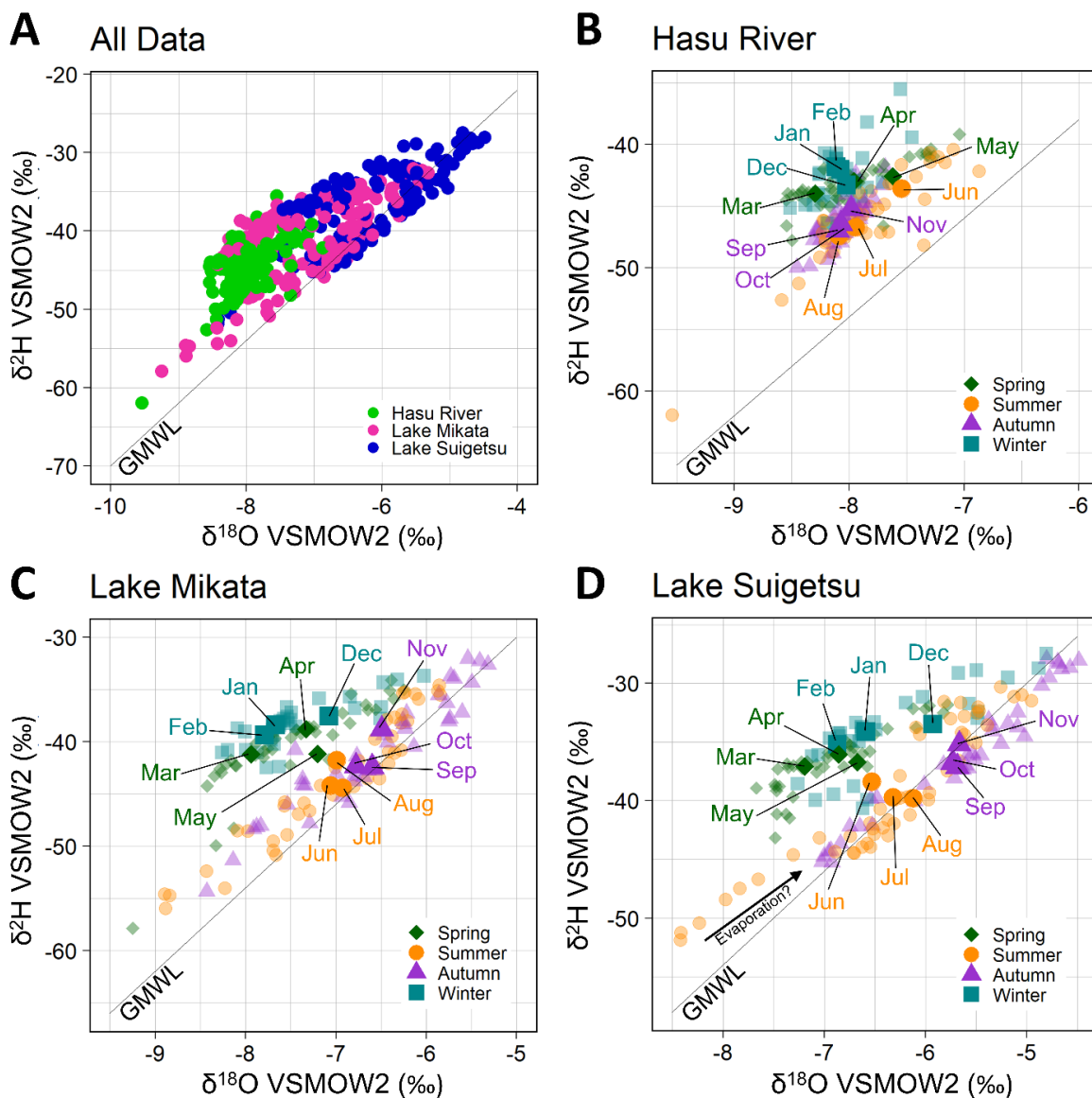
## 456 ***Catchment effects***

457           The seasonal patterns in Hasu River  $\delta_{\text{river}}$  and Lake Mikata and Lake Suigetsu surface  $\delta_{\text{lake}}$   
458 paralleled those of  $\delta_{\text{precipitation}}$ , showing that the precipitation signals were transferred to the  
459 catchment, although there is evidence for some internal modification (Figure 6). All three locations  
460 (the Hasu River, Lake Mikata and Lake Suigetsu) exhibit a smaller range of  $\delta^{18}\text{O}$  and  $\delta^2\text{H}$  values than

461 precipitation, and hence plot as a tighter grouping of points ( $\delta^{18}\text{O}$  range:  $-9.5$  to  $-4.5$  ‰ for river  
462 and lake water (Figure 6A) versus  $-13.0$  to  $-2.5$  ‰ for precipitation (Figure 3A)), which indicates  
463 homogenisation of precipitation inputs with existing catchment waters (likely both surficial water  
464 and groundwater). Whilst the isotope composition of groundwater was not quantified as part of this  
465 study, and hence remains an unknown input to the lake system, we posit that groundwater  
466 composition was merely a slower average of precipitation composition; otherwise, lake water  $\delta^{18}\text{O}$   
467 and  $\delta^2\text{H}$  would be offset to that of precipitation. We also observed that in-catchment  
468 homogenisation attenuated the effect of peripheral values and thus there was a limited influence  
469 of isolated events (including the aforementioned intense precipitation events with very low  $\delta^{18}\text{O}$   
470 and  $\delta^2\text{H}$  values) on the lake system. Instead, prolonged precipitation modes were the more  
471 dominant control. Despite annually averaged precipitation being strongly weighted to winter,  
472 signals from all four seasons were detectable in the river and lakes (discussed further below).

473         The evolution of  $\delta^{18}\text{O}$  and  $\delta^2\text{H}$  as water moves through the catchment from the Hasu River  
474 to Lake Mikata and then to Lake Suigetsu, also reveals some interesting patterns (Figure 6A). The  
475 Hasu River exhibit a very tight grouping of low isotope ratios. Isotope values then increased, parallel  
476 to the GMWL, as the water moved through to Lake Mikata and then to Lake Suigetsu. This suggests  
477 some mixing with seawater (which has higher  $\delta^{18}\text{O}$  and  $\delta^2\text{H}$ ) in the lakes, with a greater departure  
478 in values for Lake Suigetsu, which is the most saline of the three locations (discussed further below).  
479 Comparatively, the compositions of Lake Mikata and Lake Suigetsu also covered a greater range  
480 than the Hasu River. Prior to this study, it was assumed that the Hasu River was the primary input  
481 to the lakes, however the differences in the range of their isotope compositions suggests that there  
482 was an additional overland (responsive) flow component feeding the lake system and that the river  
483 received a substantial groundwater input, producing a more homogenised isotope signal (Figure 6B).  
484 Despite this, the river still reflected the seasonality of precipitation composition, and whilst monthly  
485 average composition values for the Hasu River exhibited smaller variations than Lake Mikata and

486 Lake Suigetsu, the signals from the river maintained coincident timing with these parts of the  
 487 catchment (Figure 7). These observations suggest that the Hasu River had both direct and  
 488 groundwater influences on its isotope composition, but we cannot rule out the possibility that  
 489 weekly sampling of the river did not fully capture the most extreme isotope values here, due to the  
 490 rate of river flow relative to the sampling resolution and the large catchment area.



491

492 **Figure 6: Surface water  $\delta^{18}\text{O}$  and  $\delta^2\text{H}$ .** The isotope composition of surface waters from the Hasu River, Lake Mikata  
 493 and Lake Suigetsu. Panel A shows differences in composition between parts of the catchment, with colour  
 494 corresponding to location. Subsequent panels show seasonal variations in composition at (B) the Hasu River, (C)  
 495 Lake Mikata and (D) Lake Suigetsu. In Panels B-D, monthly averages are shown as opaque symbols and labelled,  
 496 whilst underlying data points are shown as transparent symbols. Points in Panels B-D are colour-coded by season  
 497 as in Figure 3.

498

499 ***River and lake water d-excess***

500 Despite the signal homogenisation, seasonal variations in river and lake water d-excess were  
501 very similar to precipitation d-excess, with clear differences observed across the year (Figure 6B-6D)  
502 which can be interpreted in line with the precipitation signals. This offers the most convincing  
503 evidence that  $\delta_{\text{precipitation}}$  signals are detectable in  $\delta_{\text{lake}}$ . However, the difference between lake water  
504 (Figure 7) and precipitation d-excess seasonality (Figure 4) highlights a significant modification of  
505 the precipitation signals delivered to the catchment. The seasonal extremes observed in the lakes  
506 fell during spring (high d-excess) and autumn (low d-excess; Figure 7), in contrast to the winter and  
507 summer extremes observed in precipitation d-excess (Figure 4). This indicates a lag of ~1-3 months  
508 between an input of precipitation and detection of this signal in lake water composition, which we  
509 attribute to the average time taken for the water to transit through the catchment. Incidentally, this  
510 interval is equivalent to the residence time of the mixolimnion, providing support for our estimation  
511 that every three months the upper ~8m of the water column is replaced with precipitation from  
512 three months previously. A comparison of Lake Suigetsu d-excess to Wakasa precipitation d-excess  
513 suggests that the transit lag was proportional to the amount of precipitation and was longer (two  
514 to three months) for the drier summer months and shorter (one to two months) during the wetter  
515 winter months. A shorter winter lag compared to summer contrasts with what might be expected  
516 for a season associated with the accumulation of snow in the catchment (which can persist on high  
517 ground for weeks at a time) and the delayed release of snowmelt to the lakes. This appears to  
518 suggest that either the snowmelt lag was negligible compared to catchment transit time, possibly  
519 because only precipitation falling on the highest ground in the catchment was delayed, or that there  
520 was still sufficient winter rainfall or rapidly melting snow to cause a response in the lake and river  
521 water within one to two months.

522

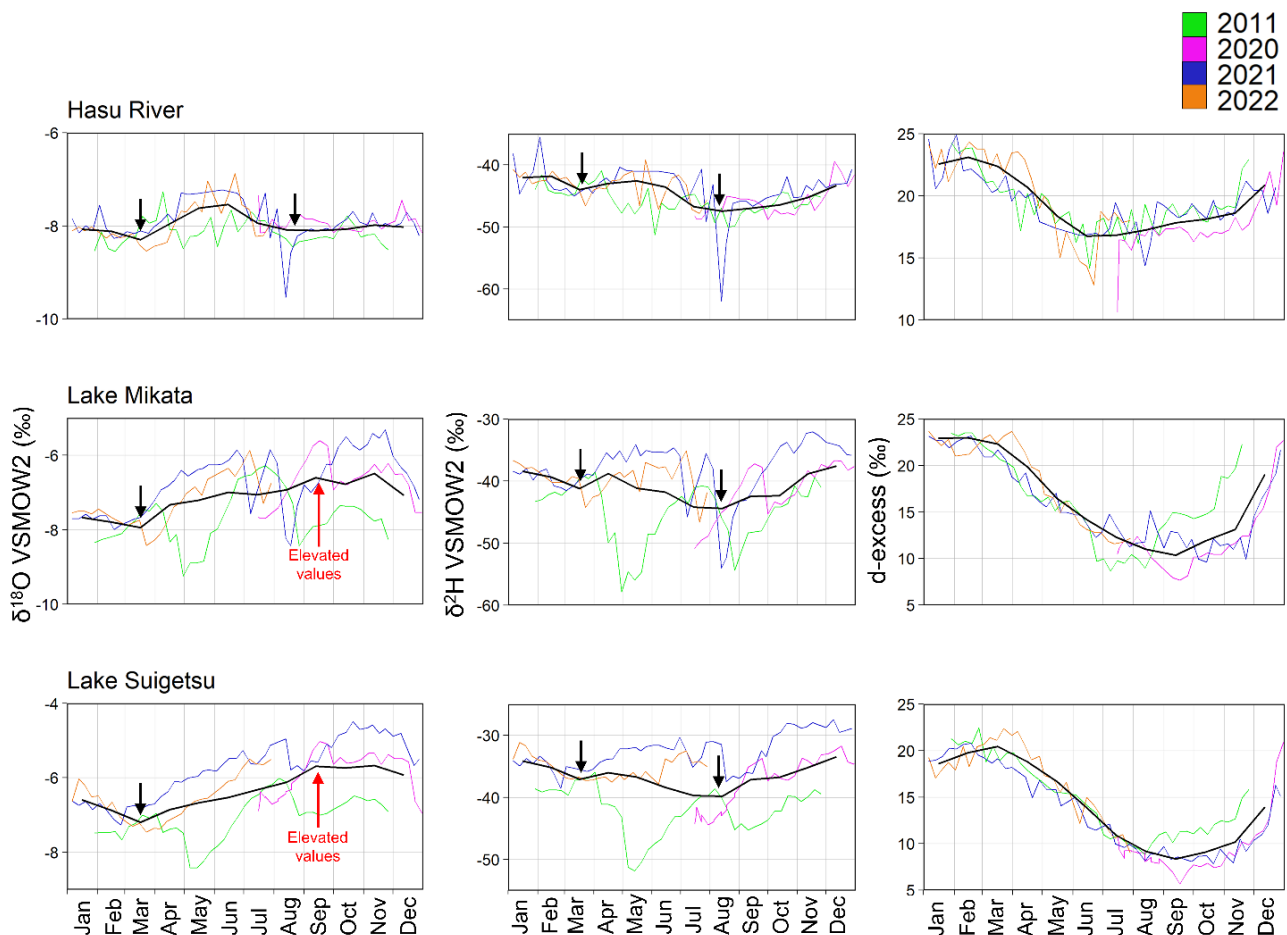


523 ***River and lake water  $\delta^{18}\text{O}$  and  $\delta^2\text{H}$***

524 The river and lake water  $\delta^{18}\text{O}$  and  $\delta^2\text{H}$  values were also very similar to precipitation,  
525 exhibiting intra-seasonal variability with significant overlap (Figure 6B-6D). The Hasu River showed  
526  $\delta^{18}\text{O}$  minima in spring and late summer, a  $\delta^2\text{H}$  minimum in late summer and slight downward  
527 inflection in  $\delta^2\text{H}$  during spring, which were reflected in both the raw datasets and in the monthly  
528 averages (Figure 7). Lake Mikata and Lake Suigetsu showed greater inter- and intra-annual  
529 differences than the Hasu River, but monthly averaged data from these parts of the catchment also  
530 exhibited minima in  $\delta^{18}\text{O}$  in the spring and  $\delta^2\text{H}$  in the late summer, as well as a downward inflection  
531 in  $\delta^2\text{H}$  during the spring (Figure 7). We relate these minima to winter (EAWM) precipitation and  
532 summer (EASM) precipitation, as detailed above in relation to precipitation  $\delta^{18}\text{O}$  and  $\delta^2\text{H}$ ;  
533 importantly, accounting for the aforementioned transit lag. However, unlike precipitation  $\delta^{18}\text{O}$ , lake  
534  $\delta^{18}\text{O}$  lacked a minimum coinciding with summer (EASM) water entering the lake; instead, there were  
535 elevated  $\delta^{18}\text{O}$  values in the autumn in Lake Suigetsu (and to a lesser extent, Lake Mikata). The  
536 autumnal  $\delta^{18}\text{O}$  peak (based on monthly averages) in Lake Suigetsu was approximately 3 ‰ greater  
537 than the  $\delta^{18}\text{O}$  of summer precipitation. We attribute this trend to a combination of lake water  
538 mixing and saline water incursion, which brings saline water with high  $\delta^{18}\text{O}$  and  $\delta^2\text{H}$  values to the  
539 surface, causing elevated lake isotope values in autumn (discussed further below) and a small  
540 amount of summer evaporative enrichment. We might also expect to see this trend in  $\delta^2\text{H}$ , given  
541 our proposed mechanisms, however this was not observed, likely as an artefact of a relatively small  
542 spring  $\delta^2\text{H}$  inflection (due to high d-excess values).

543 Besides these elevated values of lake water  $\delta^{18}\text{O}$  in summer and autumn, there is very  
544 limited evidence for an evaporation effect on the composition of lake water; a subset of summer  
545 values in each lake expressed a  $\delta^{18}\text{O}$  versus  $\delta^2\text{H}$  relationship with a reduced slope (similar to a local  
546 evaporation line), however this was restricted to the data collected in 2011 and was not present in  
547 the 2020-2022 data (Figure 6C and 6D). Additionally, the  $\delta^{18}\text{O}$  versus  $\delta^2\text{H}$  slope for other seasons

548 did not suggest evaporation effects. This highlights the potential for inter-annual variability in the  
 549 influence of evaporation on lake water isotopes, but demonstrates that this effect was a secondary  
 550 one and affected summer  $\delta^{18}\text{O}$  and  $\delta^2\text{H}$  alone. We posit that the enhanced evaporation in summer  
 551 2011 was due to lower relative humidity. Relative humidity data was not available from the local  
 552 Mihama weather station, but the nearest data from Tsuruga, 14 km to the northeast shows that  
 553 relative humidity in 2011 was on average 5 % lower than summer 2021 (Japanese Meteorological  
 554 Agency, 2023). Whilst Tsuruga experiences subtly different weather conditions, it is reasonable to  
 555 compare these locations on seasonal timescales.



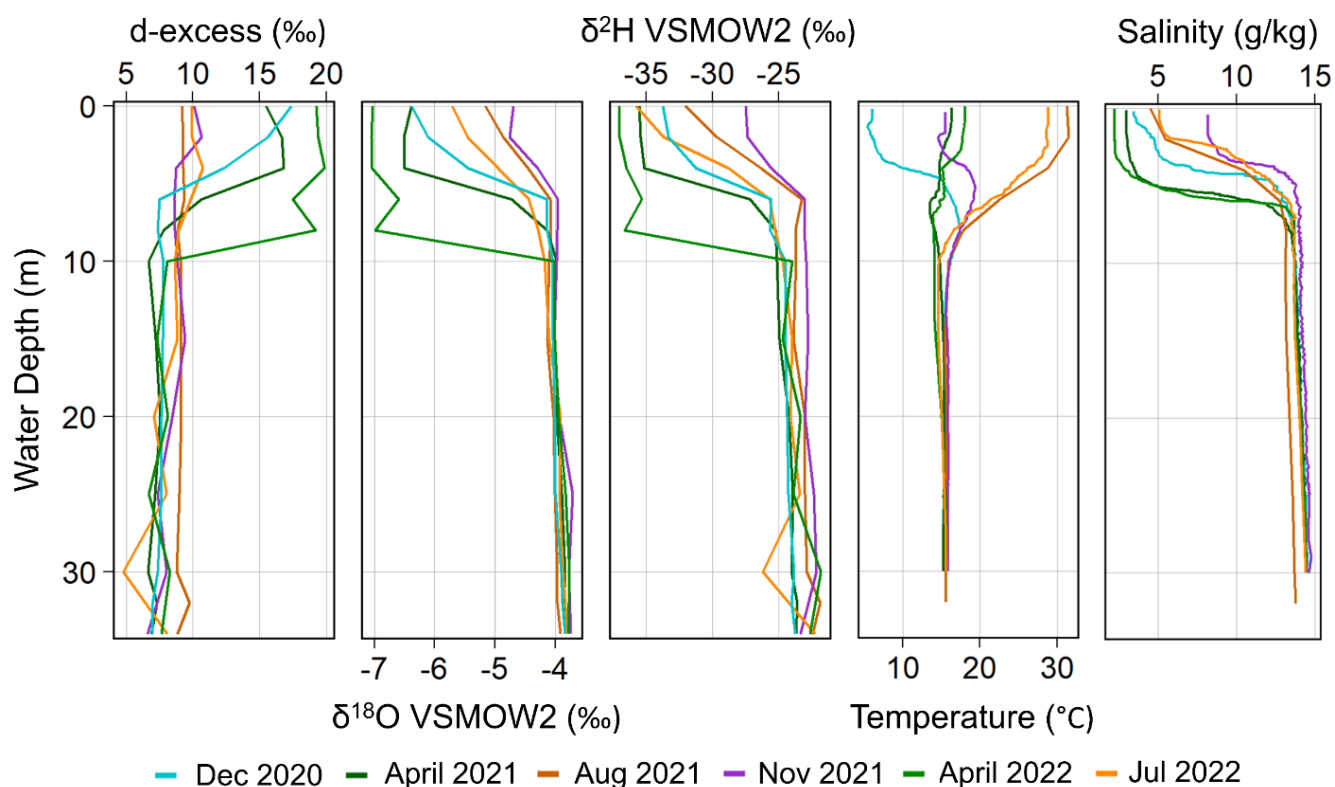
556  
 557 **Figure 7: Variations in  $\delta_{\text{river}}$  and  $\delta_{\text{lake}}$  with time.**  $\delta^{18}\text{O}$ ,  $\delta^2\text{H}$  and d-excess values from the Hasu River, Lake Mikata  
 558 and Lake Suigetsu from across the study period (colour lines). Black lines represent monthly averages of each  
 559 dataset. Vertical scales are non-equivalent to best represent the shape of the data for each location.  
 560

561 As well as this evaporation trend,  $\delta_{\text{lake}}$  in 2011 showed some discrepancies relative to the  
 562 2020-2022 interval (the data from which were broadly consistent). The data from 2011 showed a

563 distinctive trend (a minimum in  $\delta^{18}\text{O}$  and  $\delta^2\text{H}$  in May, and an earlier increase in d-excess in the  
564 autumn). Because these trends were not observed for the Hasu River, they can be attributed to  
565 within-lake processes; however, there is no comparable precipitation isotope data available for this  
566 period in order to further interrogate this interpretation. Data from the local Mihama weather  
567 station shows intense precipitation during May 2011 (448 mm), which could have resulted in a  
568 significant direct input of low  $\delta^{18}\text{O}$  and  $\delta^2\text{H}$  water into Lake Mikata and Lake Suigetsu during this  
569 month; however, with available data this remains speculative. Overall high precipitation amounts  
570 in 2011, and hence a shorter residence time, might also explain the earlier increase in lake d-excess  
571 in autumn 2011 compared to the 2020-2022 observation period.

### 572 ***Vertical profiles of lake water isotopes in Lake Suigetsu***

573 The ~quarterly depth profiling of Lake Suigetsu shows seasonal variations in the mixolimnion  
574 (above the chemocline) but compositions were consistent and homogenous in the monimolimnion  
575 year-round (Figure 8). In the monimolimnion, temperature and salinity were consistently at  $\sim 16\text{ }^\circ\text{C}$   
576 and  $\sim 14\text{ g kg}^{-1}$ , respectively. Above the chemocline, the water temperature was highest in the  
577 summer and lowest in the winter. A salinity minimum was observed during the spring and maximum  
578 during the autumn, with summer and winter exhibiting intermediate values. These observations are  
579 in agreement with the findings of Kondo *et al.* (2000), which presented long term monitoring of  
580 changes in temperature and salinity with depth at Lake Suigetsu. Throughout the sampling period  
581 the monimolimnion waters had higher  $\delta^{18}\text{O}$  and  $\delta^2\text{H}$  values relative to the mixolimnion and showed  
582 no variation with depth between  $\sim 8\text{ m}$  and the lake bottom at  $34\text{ m}$ . The d-excess values in the  
583 monimolimnion were also invariant and generally lower than the mixolimnion. In the mixolimnion,  
584 the  $\delta^{18}\text{O}$ ,  $\delta^2\text{H}$  and d-excess values showed smooth gradients between the chemocline and the  
585 surface, which suggests that the shape of each depth profile was driven by the difference between  
586 deepwater and surficial  $\delta_{\text{lake}}$ . The d-excess depth profiles in Figure 8 matched the seasonal  
587 fluctuations discussed above, with the highest values in spring and lowest values in autumn.



588

589 **Figure 8: Variations in Suigetsu  $\delta_{\text{lake}}$  with depth.** d-excess,  $\delta^{18}\text{O}$ ,  $\delta^2\text{H}$ , temperature and salinity profiles across the  
 590 study interval. Data were collected (approximately quarterly) on 22<sup>nd</sup> December 2020, 8<sup>th</sup> April 2021, 5<sup>th</sup> August  
 591 2021, 17<sup>th</sup> November 2021, 23<sup>rd</sup> April 2022 and 21<sup>st</sup> July 2022.

592

593 The  $\delta^{18}\text{O}$ ,  $\delta^2\text{H}$  and d-excess profiles did not show any correlation with temperature and  
 594 hence lake water temperature is unlikely to have been a controlling factor. However, there was an  
 595 increase in salinity,  $\delta^{18}\text{O}$  and  $\delta^2\text{H}$  through summer and autumn which suggests common drivers. We  
 596 theorise that this trend was a result of saline water incursion and mixolimnion mixing during autumn  
 597 (evidenced by Kondo *et al.*, 2020). Summer evaporation could have enhanced this effect via the  
 598 enrichment of heavier isotopes at the surface and by increasing the relative concentration of  
 599 dissolved ions. There is evidence for a combination of these effects at play, because both the  
 600 summer (August) and winter (November) profiles exhibited raised surface  $\delta^{18}\text{O}$  and  $\delta^2\text{H}$  values  
 601 (Figure 8); however, the evidence for evaporation trends in the surface water samples (discussed  
 602 above) was limited to 2011, so we suggest that in most years evaporation was less influential than  
 603 mixing. These effects explain the absence of a late summer  $\delta^{18}\text{O}$  minimum in Lake Mikata and Lake

604 Suigetsu (in contrast to precipitation  $\delta^{18}\text{O}$ ) and elevated autumn values (discussed above; Figure 7).  
605 D-excess did not appear to change significantly in autumn; possibly due to the overwhelming  
606 influence of seasonality, but most likely because the d-excess values at the surface and in the saline  
607 deep water were similar during the autumn. Hence, any amount of incursion or mixing would not  
608 result in a change in d-excess at the surface.

609         The combined influence of saline water incursion, mixing and evaporation did not persist  
610 through the entirety of the year; evidence from the surface water isotopes indicates that  
611 evaporation was limited to the summer, and extended monitoring by Kondo *et al.* (2020) suggested  
612 that mixolimnion mixing was temporally constrained to autumn. Our observations suggest that  
613 heavy winter precipitation delivered to the catchment regenerated the freshwater mixolimnion in  
614 Lake Suigetsu and effectively “reset” the effects described above, producing the minima in  $\delta^{18}\text{O}$  and  
615  $\delta^2\text{H}$  in the surface waters (Figure 7) and reinstating the relationship between precipitation and lake  
616  $\delta^{18}\text{O}$  and  $\delta^2\text{H}$ . However, since the surface waters of Lake Suigetsu retain some salinity year-round,  
617 the influence of saline water is never zero, merely diminished in relation to the effect of  
618 precipitation inputs. We observed an increase in  $\delta^{18}\text{O}$  and  $\delta^2\text{H}$  of the surface waters from the  
619 freshwater Hasu River to the fresh-brackish Lake Mikata and then to the brackish-saline Lake  
620 Suigetsu (Figure 6), which was likely due to increasing quantities of Sea of Japan-derived waters  
621 (with higher isotope compositions). The composition of Lake Suigetsu showed the greatest  
622 departure from the Hasu River composition during autumn, but there was still  $\sim 1$  ‰ difference in  
623  $\delta^{18}\text{O}$  during spring between the locations which can be attributed to this non-zero salinity. Lake  
624 Mikata existed between the compositions of Lake Suigetsu and the Hasu River because it is a  
625 shallower water body with no persistent saline deepwater but does experience a small degree of  
626 saline water incursion during autumn (Kondo *et al.*, *unpublished data*) and possibly some  
627 evaporation.

628

## 629 **Discussion**

630           The key motivation of this study was to understand the major controls of  $\delta_{\text{river}}$  and  $\delta_{\text{lake}}$  within  
631 the Five Lakes of Mikata catchment and hence direct future interpretation of isotope-based  
632 palaeoclimate proxies from the Lake Suigetsu sediment cores. Our results show that a dominant  
633 control of Lake Suigetsu  $\delta_{\text{lake}}$  (as well as Lake Mikata  $\delta_{\text{lake}}$ ) was the isotope composition of  
634 precipitation, and whilst there were internal catchment processes (homogenisation, a transit lag,  
635 seawater influences and evaporation) that affected the composition of river and lakes, for the most  
636 part (excluding autumn) these did not obscure the  $\delta_{\text{precipitation}}$  signals, or prevent their detection in  
637  $\delta_{\text{lake}}$ . Indeed, the predominant effect of the signal homogenisation was to limit the effect of  
638  $\delta_{\text{precipitation}}$  dataset noise on  $\delta_{\text{lake}}$ . In order to better understand the propagation of  $\delta_{\text{precipitation}}$  signals  
639 to  $\delta_{\text{lake}}$  across the span of the Suigetsu cores, it is important to consider the ways in which the  
640 current lake configuration is non-analogous to the past.

641           Our observations also indicate that evaporation effects were not particularly influential  
642 during the study period (with the strongest evidence limited to a single year) and were limited to  
643 the summer months. This would be expected to be the case for much of the interval covered by the  
644 Suigetsu cores, given that, aside from the Eemian, our monitoring period existed at the upper limit  
645 of temperatures experienced at the Five Lakes of Mikata for the last 150 ka. Whilst it is important  
646 to consider that evaporation is not singularly related to air temperature, but rather a range of  
647 interconnected physical processes, Lake Suigetsu receives large quantities of precipitation annually  
648 which limits the impact of evaporation on  $\delta_{\text{lake}}$  (Vystavna *et al.*, 2021). It follows that evaporation is  
649 not likely to have been a major driver of  $\delta_{\text{lake}}$  across the history of Lake Suigetsu sedimentation, as  
650 long as the region was not significantly more arid in the past, but should still be considered when  
651 interpreting proxies of summer  $\delta_{\text{lake}}$ .

652           Marine influences are also negligible from a palaeo-isotope perspective. In the modern day,  
653 saline water incursions and mixing of surface lake water with low  $\delta^{18}\text{O}$  and  $\delta^2\text{H}$  deepwater

654 originating from the Sea of Japan had a demonstrable effect on lake  $\delta^{18}\text{O}$  and  $\delta^2\text{H}$  in the autumn  
655 months. However, the connection between Lake Suigetsu and the Sea of Japan is anthropogenic  
656 and there were no marine influences on the lakes for most of the late Pleistocene (exceptions being  
657 at  $\sim 7$  ka during a highstand in the Sea of Japan, and during the Eemian global highstand) as  
658 corroborated by diatom assemblage counts of freshwater versus brackish-tolerant species (Saito-  
659 Kato *et al.*, *unpublished data*). Aside from these intervals, we predict that  $\delta_{\text{lake}}$  was not affected by  
660 seawater, either via saline water incursions or mixing. There is evidence for stratification in the past  
661 (deepwater anoxia is supported by varve preservation, and surface water oxygenation is supported  
662 by aquatic productivity); however, we would not expect to see the same stark difference in isotope  
663 compositions above and below the palaeo-chemocline as the present-day chemocline because the  
664 deepwater and surficial waters would have had the same meteoric source. As a result, there would  
665 be no influence of the Sea of Japan to Lake Suigetsu outside of these periods and the elevated  
666 autumn  $\delta^{18}\text{O}$  and  $\delta^2\text{H}$  values that partially obscure the summer precipitation  $\delta^{18}\text{O}$  minima would  
667 not be observed. Hence, in the intervals where Lake Suigetsu was a freshwater lake, we would  
668 expect  $\delta_{\text{precipitation}}$  and  $\delta_{\text{lake}}$  to be more closely aligned, and no offset between the Hasu River, Lake  
669 Mikata and Lake Suigetsu.

670           However, persistence of this stratification regime, evidenced by the preservation of varves  
671 that required basal water anoxia, suggests that the mechanistic elements of signal homogenisation  
672 (muting the seasonal precipitation signal in the surface water and homogenising the deepwater)  
673 and seasonal lags in the surface water were still active during this time, although subject to some  
674 variability. As a result, on longer timescales, palaeoclimate proxies that record deepwater  
675 conditions (e.g., isotopes of siderite ( $\text{FeCO}_3$ ), abundant in Lake Suigetsu) would record an averaged  
676  $\delta_{\text{precipitation}}$  signal, possibly over a number of years (accounting for other fractionation processes  
677 involved in signal capture by the proxy system). Conversely, palaeoclimate proxies that record  
678 surface water conditions (e.g., diatoms and other algae) will record seasonally lagged  $\delta_{\text{precipitation}}$ ; i.e.,

679 spring-weighted proxies will capture winter  $\delta_{\text{precipitation}}$ , and so forth. This relationship is of course  
680 subject to variations in the lag time (which, if lengthened, could cause greater overlap of seasonal  
681 signals) and differences in climate, which could alter the timing of delivery to the lakes. During glacial  
682 intervals, pollen reconstructed temperature for the coldest month is consistently below 0 °C,  
683 suggesting that the limited snowmelt lag in the present day would be more prominent. Additionally,  
684 the lakes were likely frozen on the surface for much of the winter. Overall, this would be expected  
685 to have stalled the movement of water through the catchment and extend the transit lag between  
686 delivery of winter (EAWM) precipitation and detection in the lake into the spring season. Under  
687 these circumstances, palaeoclimate proxies that capture the spring  $\delta_{\text{lake}}$ , such as spring blooming  
688 diatoms, would capture winter (EAWM)  $\delta_{\text{precipitation}}$  (arguably with even greater certainty than the  
689 present day). Proxies that capture summer  $\delta_{\text{lake}}$ , such as algal biomarkers would, by contrast,  
690 capture a mix between winter, spring and summer  $\delta_{\text{precipitation}}$  because these would enter the lake in  
691 quicker succession (although spring precipitation quantities are very small in comparison to winter  
692 and summer, and hence are unlikely to have a significant effect). Autumn  $\delta_{\text{lake}}$ -capturing proxies,  
693 such as autumn blooming diatoms, would still predominately capture summer (EASM)  $\delta_{\text{precipitation}}$   
694 composition. Terrestrial proxies (e.g.,  $\delta^{18}\text{O}$  of pollen grains and  $\delta^2\text{H}$  of long-chained n-alkanes and  
695 n-alkanoic acids) would be unaffected by changes to the transit lag as they capture soil pore water  
696 rather than lake water and would be expected to more closely reflect changing  $\delta_{\text{precipitation}}$ .

697         Having established that the dominant driver of  $\delta_{\text{lake}}$  is  $\delta_{\text{precipitation}}$ , it is prudent to consider  
698 what could affect this quantity in the past. We anticipate that palaeo-EAM precipitation from both  
699 seasonal modes was a dominant influence on  $\delta_{\text{precipitation}}$  delivered to the catchment because winter  
700 and summer are associated with large quantities of precipitation (and hence  $\delta_{\text{precipitation}}$  will be  
701 weighted towards the composition of the EAWM and EASM). Additionally, whilst autumn  
702 (predominately typhoon) precipitation provides a third period of rain annually, and we observe the  
703 influence of intense precipitation events on  $\delta^{18}\text{O}$  and  $\delta^2\text{H}$  of precipitation, these signals were not



704 detected in the lakes. For this reason, we anticipate that unless typhoon frequency was significantly  
705 greater in the past, the tendency of  $\delta_{\text{lake}}$  to reflect only extended seasonal precipitation events (i.e.,  
706 the EAM) will limit the influence of typhoon precipitation, even if it is recorded in  $\delta_{\text{precipitation}}$ . It is not  
707 unreasonable, therefore, to exclude the typhoon season influence on  $\delta_{\text{precipitation}}$ , and consider  
708  $\delta_{\text{precipitation}}$  at Wakasa to be most closely linked with EAM behaviour. Importantly, the influence of  
709 both EAWM and EASM components were observed at the catchment, establishing that the area is  
710 a sensitive location – even optimised, especially relative to Tokyo – for studying both components  
711 of the EAM. This is particularly useful given the skew in existing palaeoclimate reconstructions  
712 towards the summer months.

713           However, our findings were consistent with others from central Japan (e.g., Taniguchi *et al.*,  
714 2000), which note that for contemporary isotopes there is no significant difference in  $\delta^{18}\text{O}$  and  $\delta^2\text{H}$   
715 between EAWM and EASM precipitation. As such, it is important to note that unlike Continental  
716 Asia, annually integrated  $\delta^{18}\text{O}$  and  $\delta^2\text{H}$  do not reflect the changing relative input of EAWM and EASM  
717 precipitation, because their compositions are so alike. Isotope composition averaged on  
718 multiannual timescales will not reflect the balance between these systems unless either one of  
719 EAWM or EASM changes in strength and the other remains stable, or one increases in strength and  
720 the other decreases concurrently. These changes in behaviour can be caused by different climatic  
721 regimes (such as glacial periods) or across climatic transitions. Under such conditions, the changing  
722 strength of the EAWM and EASM would be expected to impact on both the annually averaged deep  
723  $\delta_{\text{lake}}$  and the seasonally-lagged surface water  $\delta_{\text{lake}}$ ; the former by affecting the balance between the  
724 two seasonal modes, and the latter by affecting either EAWM or EASM  $\delta_{\text{precipitation}}$ . Under these  
725 circumstances, EAWM and EASM  $\delta_{\text{precipitation}}$  would diverge, and hence terrestrial and surface water  
726 palaeoclimate proxy seasonality becomes extremely important for interpretation. It is therefore  
727 vital to know which composition (winter-weighted, summer-weighted or mixed) is captured by each  
728 palaeoclimate proxy before interpreting the signal, accounting also for changes to the lag time.

729 Our observations are restricted to the study interval, and hence provide limited  
730 contributions to the interpretation of long-term drivers of  $\delta^{18}\text{O}$  and  $\delta^2\text{H}$  associated with EAM  
731 behaviour, however this remains an important component of palaeoclimate proxy interpretation.  
732 EAM rainfall  $\delta_{\text{precipitation}}$  tends to respond inversely to monsoon strength, due to a combination of  
733 preferential rainout of the heavier isotopes, enhanced by increased quantities of precipitation and  
734 increased cloud top height with a stronger monsoonal convection, which is associated with low  
735 condensation temperatures (Cai and Tian, 2016). Our results show that the amount effect does not  
736 have a strong relationship within the catchment in the modern day; however, that does not preclude  
737 a relationship to monsoon intensity; Uemura *et al.* (2012) noted a limited influence of local  
738 precipitation amount on  $\delta^{18}\text{O}$  in Okinawa (Southern Japan), but that the precipitation amount  
739 integrated over the full transport pathway was significant. Furthermore, the Fukugaguchi stalagmite  
740 record (Itoigawa, central Japan) shows a strong relationship of  $\delta^{18}\text{O}$  to EAWM precipitation amount  
741 despite modern  $\delta_{\text{precipitation}}$  showing a statistically weak relationship to precipitation amount (Sone  
742 *et al.*, 2013). Other factors which could contribute to the overall signal are changes at source:  
743 composition, temperature and relative humidity (e.g., Amekawa *et al.*, 2021), and, in the EASM  
744 mode, the positioning of the EAM front (Kurita *et al.*, 2015). Furthermore, the prevalence of sea ice  
745 during glacial periods, particularly in the relatively isolated Sea of Japan, might be expected to limit  
746 evaporation despite changes to EAWM strength. Hence, it is vital to consider how EAM  $\delta_{\text{precipitation}}$   
747 was controlled by the evolution of the climate of the region as a whole and how this affected  
748  $\delta_{\text{precipitation}}$  at Wakasa.

749 Finally, the clearest seasonal signal derived from the catchment was undoubtedly that of d-  
750 excess, and this was the only isotope parameter which demonstrated the ability to distinguish  
751 precipitation from different seasons. Not only this, but the transfer of the d-excess signal from  
752 precipitation to lake was clearer than for  $\delta^{18}\text{O}$  and  $\delta^2\text{H}$ , possibly due to the amplitude of seasonal  
753 changes and the limited influence of other competing controls. However, it is much more difficult

754 to calculate d-excess using palaeo-isotope reconstructions, because it requires the combination of  
755 temporally and spatially equivalent  $\delta^{18}\text{O}$  and  $\delta^2\text{H}$  values. If compatible palaeoclimate proxy records  
756 are produced and d-excess calculation becomes possible, this should be a consideration for future  
757 research based on the excellent seasonal distinctions observed in this variable and its potential as a  
758 powerful proxy of past monsoon dynamics.

759

## 760 **Conclusions**

761 Understanding the relationship between climate variability, the isotope composition of  
762 precipitation and the transfer of precipitation isotope signals into lake waters is essential to support  
763 the interpretation of past climates using isotope-based proxies derived from lake sediments. Using  
764 contemporary monitoring of the isotope composition of precipitation ( $\delta_{\text{precipitation}}$ ), river water ( $\delta_{\text{river}}$ )  
765 and lake water ( $\delta_{\text{lake}}$ ) across the Five Lakes of Mikata catchment, Japan, we assessed the factors  
766 affecting  $\delta_{\text{lake}}$ , with a particular focus on Lake Suigetsu. Precipitation  $\delta^{18}\text{O}$  and  $\delta^2\text{H}$  exhibited only  
767 small seasonal differences across the year due to the similar compositions of winter (EAWM) and  
768 summer (EASM) precipitation, which act as end members with opposing trajectories. Precipitation  
769 d-excess, by contrast, clearly demarcated the different seasonal influences due to different  
770 evaporation conditions at the moisture sources of the EAWM (Sea of Japan) and EASM (Pacific  
771 Ocean domain), with a gradual shift between the two during the spring and autumn. The difference  
772 between winter and summer d-excess was enhanced by the location of the catchment. There was  
773 limited statistical evidence to support a temperature effect over precipitation  $\delta^{18}\text{O}$  or  $\delta^2\text{H}$ ; however,  
774 when considering the data on a seasonal basis, there was some evidence to support a local amount  
775 effect, with minima in monthly averaged  $\delta^{18}\text{O}$  and  $\delta^2\text{H}$  during the wettest (EAM) seasons of the year.

776 We found that  $\delta_{\text{lake}}$  and  $\delta_{\text{precipitation}}$  were directly related, although the spread of values of  
777  $\delta_{\text{lake}}$  was more limited due to in-catchment homogenisation. Despite this, compositional patterns  
778 were preserved, and it was still possible to detect seasonal trends in  $\delta_{\text{lake}}$ , which paralleled those of

779  $\delta_{\text{precipitation}}$  and were attributed to the same causes. A two to three-month transit lag between  
780  $\delta_{\text{precipitation}}$  and  $\delta_{\text{lake}}$  was observed and the length of this lag related to the quantity of precipitation.  
781 The influence of isolated precipitation events on  $\delta_{\text{lake}}$  (including typhoons) was negligible in  
782 comparison to significant extended freshwater inputs to the catchment from the East Asian  
783 Monsoon. The incursion of saline water from the Sea of Japan and autumnal mixing resulted in  
784 elevated  $\delta^{18}\text{O}$  and  $\delta^2\text{H}$  values in the lakes during late summer and autumn (obscuring the  $\delta^{18}\text{O}$   
785 minimum equated to the EASM) and caused a greater effect for Lake Suigetsu than Lake Mikata.  
786 This was possibly combined with summer evaporation effects, although evidence for the influence  
787 of evaporation varied between years. The large influx of winter precipitation to the catchment re-  
788 established the relationship between  $\delta_{\text{lake}}$  and  $\delta_{\text{precipitation}}$  which extended from winter to early  
789 summer. Deep water composition in Lake Suigetsu was stable and homogenous across the study  
790 period.

791 These results will facilitate interpretation of palaeoclimate reconstructions derived from  
792 oxygen and hydrogen isotope analysis of the Lake Suigetsu sediment cores. It is expected that  
793  $\delta_{\text{precipitation}}$  (and thus  $\delta_{\text{lake}}$ ) will be closely related to East Asian Summer Monsoon and East Asian  
794 Winter Monsoon  $\delta_{\text{precipitation}}$  fluctuations across the  $\sim 150$  ka of the late Quaternary covered by the  
795 Suigetsu cores. The seasonal patterns in  $\delta_{\text{lake}}$  could be altered under different climatic regimes by  
796 large scale drivers (such as monsoon strength and balance of seasonal precipitation), along with the  
797 influence of local factors, including the transit lag. However, not all of the factors affecting  $\delta_{\text{lake}}$   
798 observed during this contemporary monitoring will be significant on longer timescales. The  
799 incursion of sea water is a consequence of anthropogenic catchment alteration and, as such, is not  
800 expected to have affected the lake water isotope hydrology prior to the last  $\sim 400$  years. Evaporation  
801 is also expected to have minimal effects on down-core  $\delta_{\text{lake}}$  reconstructions which are limited to the  
802 summer months. Robust interpretation is predicated on sound understanding of proxy seasonality  
803 and whether the proxy captures surficial or deepwater  $\delta_{\text{lake}}$ .

804

## 805 **Acknowledgements and Funding**

806 The authors would like to thank T. Tanabe for their contribution to collecting the water samples in  
807 2011-2012, K. Ichiyanagi and M. Tanoue for permission to use their precipitation isotope data from  
808 Tokyo and R. Kondo for access to contemporary salinity data for the Five Lakes of Mikata. All other  
809 isotope analysis was conducted by C. Arrowsmith; J. Lacey contributed to the writing of the  
810 methodology section; and M. Ankor designed and built the rainwater sampler. Water quality data  
811 for the water column of Suigetsu Lake were provided by Dr Yasushi Miyamoto. This research was  
812 financially supported by an Australian Research Council Discovery Project (DP200101768), a JSPS  
813 KAKENHI Grant (19K20442) and C.L.Rex was supported by the NERC IAPETUS2 Doctoral Training  
814 Partnership. The authors declare no conflicts of interest.

815

## 816 **Data Availability**

817 Datasets related to this article can be found at [10.5525/gla.researchdata.1429](https://doi.org/10.5525/gla.researchdata.1429), hosted at University  
818 of Glasgow.

819

## 820 **Appendix 1- Sampling locations**

821 Details of sampling locations noted in the text and on Figure 1, with notes relating to when each location was used.

| Sampling Location           | Coordinates               | Location Code | Notes  |
|-----------------------------|---------------------------|---------------|--|
| <b>Hasu River (2011-12)</b> | 35°33'07"N<br>135°54'03"E | HASU11        |  |
| <b>Mikata (2011-12)</b>     | 35°34'18"N<br>135°52'05"E | MIKATA11      |  |
| <b>Suigetsu (2011-12)</b>   | 35°34'59"N<br>135°52'08"E | SUIGETSU11    |  |
| <b>Mikata (2020-22)</b>     | 35°33'33"N<br>135°52'58"E | MIKATA20A     | (Unless inaccessible - usually due to heavy rain and high lake levels) |
| <b>Mikata 2 (2020-22)</b>   | 35°33'38"N<br>135°52'49"E | MIKATA20B     | (When Mikata was inaccessible)   |
| <b>Mikata 3 (2020-22)</b>   | 35°34'01"N<br>135°52'10"E | MIKATA20C     | (When Mikata and Mikata 2 were inaccessible)                           |

|   |                           |                |  |
|---|---------------------------|----------------|--|
| <b>Hasu River Tana Bridge (2020-22)</b> | 35°32'40"N<br>135°54'04"E | HASUTANA20     | (Unless blocked for renovations)                               |
| <b>Hasu River Sako Bridge (2020-22)</b> | 35°32'10"N<br>135°53'59"E | HASUSAKO20     | (When Hasu Tana Bridge was blocked for renovations)            |
| <b>Suigetsu Peninsula (2020-22)</b>     | 35°35'17"N<br>135°52'34"E | SUIGETSUPEN20A | (Until 18 Aug 2020 - moved due to algal growth)                |
| <b>Suigetsu Peninsula (2020-22)</b>     | 35°35'22"N<br>135°52'40"E | SUIGETSUPEN20B | (Since 26 Aug 2020, unless inaccessible - usually due to snow) |
| <b>Suigetsu Bay (2020-22)</b>           | 35°35'25"N<br>135°52'02"E | SUIGETSUBAY20  | (When Suigetsu Peninsula was inaccessible)                     |
| <b>Suigetsu Roadside (2020-22)</b>      | 35°35'04"N<br>135°52'05"E | SUIGETSUROAD20 | (Not used as of 05/01/22)                                      |
| <b>Suigetsu Column (2020-22)</b>        | 35°35'05"N<br>135°53'01"E | SUIGETSUCOL20  | (approx. - better described as the centre of the lake)         |
| <b>Netatmo Weather Station</b>          | 35°33'32"N<br>135°53'48"E | WEATHER20      |  |
| <b>Precipitation (2020-22)</b>          | 35°33'43"N<br>135°53'25"E | RAINFALL20     |  |

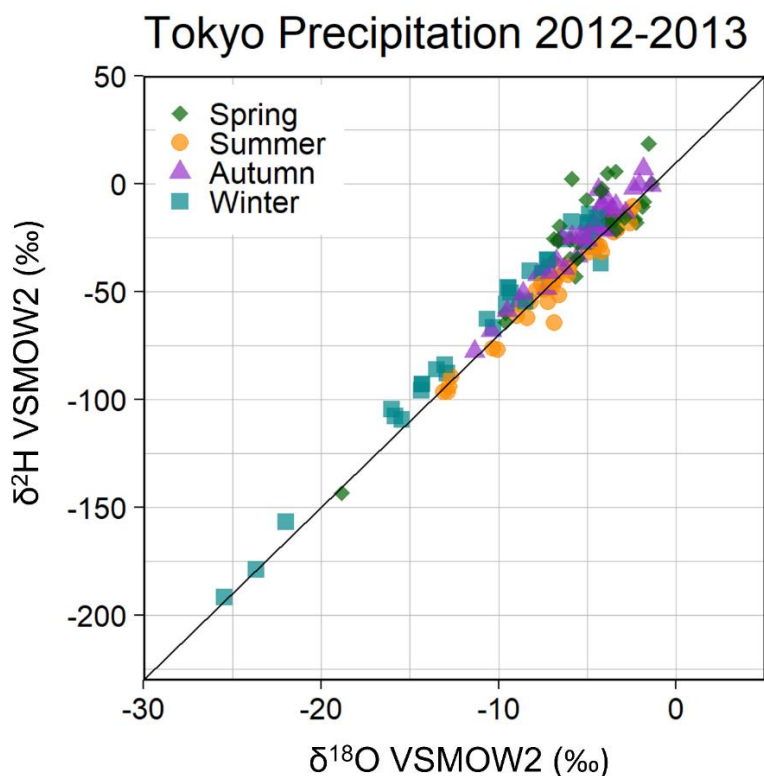
822

823 **Appendix 2- Least-squares linear regression analysis**

824 Coefficients of determination ( $R^2$ ) between  $\delta^{18}\text{O}$  and  $\delta^2\text{H}$  in precipitation, square root transformed total  
825 precipitation during the collection period, and average temperature during the collection period. Least-squares  
826 linear regression slopes and intercepts are also provided.

|                                     | Total Precipitation (square root transformed) |       |           | Average Temperature |       |           |
|-------------------------------------|---|-------|-----------|---------------------|-------|-----------|
|                                     | $R^2$   | Slope | Intercept | $R^2$               | Slope | Intercept |
| $\delta^{18}\text{O}$ (all data)    | 0.18  | -0.38 | -4.94     | 0.01                | 0.03  | -7.39     |
| $\delta^2\text{H}$ (all data)       | 0.06  | -2.06 | -25.45    | 0.09                | -0.81 | -25.73    |
| $\delta^{18}\text{O}$ (spring only) | 0.18  | -0.47 | -3.91     | 0.07                | -0.15 | -4.32     |
| $\delta^2\text{H}$ (spring only)    | 0.19  | -4.31 | -17.64    | 0.23                | -2.37 | -9.17     |
| $\delta^{18}\text{O}$ (summer only) | 0.34  | -0.45 | -5.31     | 0.07                | 0.20  | -12.71    |
| $\delta^2\text{H}$ (summer only)    | 0.26  | -3.3  | -37.55    | 0.12                | 2.18  | -109.30   |
| $\delta^{18}\text{O}$ (autumn only) | 0.30  | -0.64 | -3.44     | 0.06                | 0.12  | -8.89     |
| $\delta^2\text{H}$ (autumn only)    | 0.20  | -4.49 | -12.54    | 0.00                | -0.24 | -30.32    |
| $\delta^{18}\text{O}$ (winter only) | 0.00  | -0.04 | -7.33     | 0.18                | 0.26  | -8.97     |
| $\delta^2\text{H}$ (winter only)    | 0.00  | 1.13  | -35.72    | 0.04                | 1.13  | 35.72     |

827



829

830 **Isotopes in precipitation for Tokyo, 2013.** Based on event-based sampling in Arakawa and Meguro districts, Tokyo  
 831 Prefecture (Ichiyanagi and Tanoue, 2016). Similarities between this dataset and the equivalent Tokyo dataset in  
 832 Figure 3B demonstrate the robustness of comparison between the Tokyo GNIP dataset and the isotopes in  
 833 precipitation at Wakasa (this study).

834

835 The similarities between the event-based precipitation isotope data from Tokyo shown  
 836 below (Ichiyanagi and Tanoue, 2016) and the longer term monthly Global Network of Isotopes in  
 837 Precipitation (GNIP) data from 1960-1979 demonstrate the robustness of comparisons made  
 838 between the Wakasa precipitation data (2020-22) and the Tokyo GNIP data. In particular, this shows  
 839 that the differences observed between precipitation isotopes in Wakasa and Tokyo cannot be  
 840 attributed to differences in climate between 1960-79 and the present day. The data presented  
 841 below (from 2013) are more scattered than the Tokyo GNIP data (likely a result of a short sampling  
 842 period) but retain the same summer and winter end members which closely overlap due to similar  
 843 d-excess values. Furthermore, these data demonstrate that considering monthly averages, rather

844 than shorter-term (event based) values simply removes excess scatter from the dataset and does  
845 not eliminate seasonal patterns.

846

## 847 References

848 Amekawa, S. Kashiwagi, K., Hori, M., Sone, T., Kato, H., Okumura, T., Yu, T.L., Shen, C.C., Kano, A.  
849 (2021). Stalagmite evidence for East Asian winter monsoon variability and 18O-depleted  
850 surface water in the Japan Sea during the last glacial period. *Progress in Earth and Planetary*  
851 *Science*, **8**(1). doi: 10.1186/s40645-021-00409-8.

852 Araguás-Araguás, L., Froehlich, K., and Rozanski, K. (1998). Stable isotope composition of  
853 precipitation over southeast Asia. *Journal of Geophysical Research Atmospheres*, **103**(D22),  
854 28721–28742. doi: 10.1029/98JD02582

855 Bershaw J. (2018). Controls on Deuterium Excess across Asia. *Geosciences*, **8**(7), 257. doi:  
856 10.3390/geosciences8070257

857 Bronk Ramsey, C., Staff, R. A., Bryant, C. L., Brock, F., Kitagawa, H., Van Der Plicht, J., Scholaut, G.,  
858 Marshall, M. H., Brauer, A., Lamb, H. F., Payne, R. L., Tarasov, P. E., Haraguchi, T., Gotanda,  
859 K., Yonenobu, H., Yokoyama, Y., Tada, R., and Nakagawa, T. (2012). A complete terrestrial  
860 radiocarbon record for 11.2 to 52.8 kyr B.P. *Science*, **338**(6105), 370–374. doi:  
861 10.1126/science.1226660

862 Bronk Ramsey, C., Heaton, T. J., Scholaut, G., Staff, R. A., Bryant, C. L., Brauer, A., Lamb, H. F.,  
863 Marshall, M. H., and Nakagawa, T. (2020). Reanalysis of the Atmospheric Radiocarbon  
864 Calibration Record from Lake Suigetsu, Japan. *Radiocarbon*, **62**(4), 989–999. doi:  
865 10.1017/RDC.2020.18

866 Esri (2022a). “World Dark Grey Base” [basemap] 1:10,000,000 (panel A), 1:400,000 (panel B),  
867 1:67,946 (panel C).



868 <https://www.arcgis.com/home/item.html?id=a284a9b99b3446a3910d4144a50990f6>  
869 (accessed 12/09/2022).

870 Esri (2022b). “World Hillshade” [basemap] 1:10,000,000 (panel A), 1:400,000 (panel B), 1:67,946  
871 (panel C).  
872 <https://www.arcgis.com/home/item.html?id=1b243539f4514b6ba35e7d995890db1d>  
873 (accessed 12/09/2022).

874 Fudeyasu, H., Ichiyanagi, K., Sugimoto, A., Yoshimura, K., Ueta, A., Yamanaka, M. D., and Ozawa, K.  
875 (2008). Isotope ratios of precipitation and water vapor observed in Typhoon Shanshan.  
876 *Journal of Geophysical Research Atmospheres*, **113**, article D12113. doi:  
877 10.1029/2007JD009313

878 Gallagher, S. J., Sagawa, T., Henderson, A. C. G., Saavedra-Pellitero, M., De Vleeschouwer, D., Black,  
879 H., Itaki, T., Toucanne, S., Bassetti, M. A., Clemens, S., Anderson, W., Alvarez-Zarikian, C., and  
880 Tada, R. (2018). East Asian Monsoon History and Paleoceanography of the Japan Sea Over  
881 the Last 460,000 Years. *Paleoceanography and Paleoclimatology*, **33**(7), 683–702. doi:  
882 10.1029/2018PA003331

883 Gibson, J. J., Birks, S. J., and Yi, Y. (2016). Stable isotope mass balance of lakes: A contemporary  
884 perspective. *Quaternary Science Reviews*, **131**, 316–328. doi:  
885 10.1016/j.quascirev.2015.04.013

886 Gonfiantini, R. (1986). Environmental isotopes in lake studies. In: Fritz, P. and Fontes, J.C. eds.  
887 Handbook of environmental isotope geochemistry volume two, the terrestrial environment,  
888 B. Netherlands: Elsevier, 113-168. doi: 10.1016/B978-0-444-42225-5.50008-5

889 Hasegawa, H., Akata, N., Kawabata, H., Sato, T., Chikuchi, Y., and Hisamatsu, S. (2014).  
890 Characteristics of hydrogen and oxygen stable isotope ratios in precipitation collected in a  
891 snowfall region, Aomori Prefecture, Japan. *Geochemical Journal*, **48**(1), 9–18. doi:  
892 10.2343/geochemj.2.0279

893 Ichiyanagi, K., Tanoue, M. and on behalf of the Isotope Mapping Working Group of the Japanese  
894 Society of Hydrological Science (IMWG/JAHS) (2016). Spatial analysis of annual mean stable  
895 isotopes in precipitation across Japan based on an intensive observation period throughout  
896 2013. *Isotopes in Environmental and Health Studies*, **52**(4–5), 353–362. doi:  
897 10.1080/10256016.2015.1132215

898 Ichiyanagi, K., and Tanoue, M. (2016). Stable isotopes in precipitation across Japan during an  
899 intensive observation period throughout 2013. *Journal of Japanese Association of*  
900 *Hydrological Sciences*, **46**(2), 123–138. doi: 10.4145/jahs.46.123

901 Jackisch, D., Yeo, B. X., Switzer, A. D., He, S., Cantarero, D. L. M., Siringan, F. P., and Goodkin, N. F.  
902 (2022). Precipitation stable isotopic signatures of tropical cyclones in Metropolitan Manila,  
903 Philippines, show significant negative isotopic excursions. *Natural Hazards and Earth System*  
904 *Sciences*, **22**(1), 213–226. doi: 10.5194/nhess-22-213-2022

905 Japanese Meteorological Agency (2022). Mihama (Fukui Prefecture) JMA Weather Station Data,  
906 electronic dataset, Japanese Meteorological Agency, viewed 10/02/2022,  
907 <<https://www.data.jma.go.jp/risk/obsdl/index.php>>

908 Japanese Meteorological Agency (2023). Tsuruga (Fukui Prefecture) JMA Weather Station Data,  
909 electronic dataset, Japanese Meteorological Agency, viewed 23/06/2023,  
910 <<https://www.data.jma.go.jp/risk/obsdl/index.php>>

911 Jasechko, S., Birks, S.J., Gleeson, T., Wada, Y., Fawcett, P.J., Sharp, Z.D., McDonnell, J.J. and Welker,  
912 J.M. (2014). The pronounced seasonality of global groundwater recharge. *Water Resources*  
913 *Research*, **50**(11), 8845-8867. doi: 10.1002/2014WR015809

914 Jun-Mei, L., Jian-Hua, J. and Shi-Yan, T. (2013). Re-Discussion on East Asian Meiyu Rainy Season.  
915 *Atmospheric and Oceanic Science Letters*, **6**, 279–283. doi: 10.3878/j.issn.1674-  
916 2834.13.0024

917 Kondo, R., and Butani, J. (2007). Comparison of the diversity of sulfate-reducing bacterial  
918 communities in the water column and the surface sediments of a Japanese meromictic lake.  
919 *Limnology*, **8**, 131–141. doi: 10.1007/s10201-007-0201-9

920 Kondo, R., Kasashima, N., Matsuda, H., and Hata, Y. (2000). Determination of thiosulfate in a  
921 meromictic lake. *Fisheries Science*, **66**(6), 1076–1081. doi: 10.1046/j.1444-  
922 2906.2000.00171.x

923 Kondo, R., Kodera, M., Mori, Y., Okamura, T., Yoshikawa, S., and Ohki, K. (2014). Spatiotemporal  
924 distribution of bacteriochlorophylls in the meromictic Lake Suigetsu, Japan. *Limnology*, **15**,  
925 77–83. doi: 10.1007/s10201-013-0415-y

926 Kurita, N., Fujiyoshi, Y., Nakayama, T., Matsumi, Y. and Kitagawa, H. (2015) East Asian Monsoon  
927 controls on the inter-annual variability in precipitation isotope ratio in Japan. *Climate of the*  
928 *Past*, **11**, 339–353. doi: 10.5194/cp-11-339-2015.

929 Lawrence, R.J. and Gedzelman, D.S., (1996). Low stable isotope ratios of tropical cyclone rains.  
930 *Geophysical Research Letters*, **23**(5), 527–530. doi: 10.1029/96GL00425

931 Li, C., Kano, N., Ueno, Y., Hanabusa, M., Jiao, Y., Imaizumi, H., and Watanabe, N. (2010).  
932 Characteristics of Oxygen Stable Isotopic Ratio in Precipitations in Niigata Prefecture, Japan.  
933 *Radioisotopes*, **59**(2), 93–102. doi: 10.3769/radioisotopes.59.93

934 Masuzawa, T., and Kitano, Y. (1982). Diagenetic deposition of manganese in sediment of a  
935 historically meromictic lake, Lake Suigetsu, Japan. *Journal of the Oceanographical Society of*  
936 *Japan*, **38**, 73–80. doi: 10.1007/BF02110293

937 Matsuyama, M. (1973). Changes in the Limnological Features of a Meromictic Lake Suigetsu during  
938 the Years, 1926–1967. *Journal of Oceanography*, **29**, 131–139. doi: 10.1007/BF02109088

939 Matsuyama, M. (1974). Vertical distributions of some chemical substances in surface sediments of  
940 a meromictic Lake Suigetsu. *Journal of the Oceanographical Society of Japan*, **30**, 209–215.  
941 doi: 10.1007/BF02111046

942 McLean, D., Albert, P. G., Nakagawa, T., Staff, R. A., Suzuki, T., and Smith, V. C. (2016). Identification  
943 of the Changbaishan 'Millennium' (B-Tm) eruption deposit in the Lake Suigetsu (SG06)  
944 sedimentary archive, Japan: Synchronisation of hemispheric-wide palaeoclimate archives.  
945 *Quaternary Science Reviews*, **150**, 301–307. doi: 10.1016/j.quascirev.2016.08.022

946 Nakagawa, T., Gotanda, K., Haraguchi, T., Danhara, T., Yonenobu, H., Brauer, A., Yokoyama, Y., Tada,  
947 R., Takemura, K., Staff, R. A., Payne, R. L., Bronk Ramsey, C., Bryant, C. L., Brock, F., Scholout,  
948 G., Marshall, M. H., Tarasov, P. E., and Lamb, H. F. (2012). SG06, a fully continuous and varved  
949 sediment core from Lake Suigetsu, Japan: Stratigraphy and potential for improving the  
950 radiocarbon calibration model and understanding of late Quaternary climate changes.  
951 *Quaternary Science Reviews*, **36**, 164–176. doi: 10.1016/j.quascirev.2010.12.013

952 Nakagawa, T., Tarasov, P., Staff, R., Bronk Ramsey, C., Marshall, M., Scholout, G., Bryant, C., Brauer,  
953 A., Lamb, H., Haraguchi, T., Gotanda, K., Kitaba, I., Kitagawa, H., van der Plicht, J., Yonenobu,  
954 H., Omori, T., Yokoyama, Y., Tada, R., and Yasuda, Y. (2021). The spatio-temporal structure  
955 of the Lateglacial to early Holocene transition reconstructed from the pollen record of Lake  
956 Suigetsu and its precise correlation with other key global archives: Implications for  
957 palaeoclimatology and archaeology. *Global and Planetary Change*, **202**, 103493. doi:  
958 10.1016/j.gloplacha.2021.103493

959 Rolph, G., Stein, A. and Stunder, B. (2017). Real-time Environmental Applications and Display sYstem:  
960 READY. *Environmental Modelling and Software*, **95**, 210–228. doi:  
961 10.1016/j.envsoft.2017.06.025

962 Russell, J. M., and Johnson, T. C. (2006). The water balance and stable isotope hydrology of Lake  
963 Edward, Uganda-Congo. *Journal of Great Lakes Research*, **32**(1), 77–90. doi: 10.3394/0380-  
964 1330(2006)32[77:TWBASI]2.0.CO;2

965 Scholout, G., Marshall, M. H., Brauer, A., Nakagawa, T., Lamb, H. F., Staff, R. A., Bronk Ramsey, C.,  
966 Bryant, C. L., Brock, F., Kossler, A., Tarasov, P. E., Yokoyama, Y., Tada, R., and Haraguchi, T.

967 (2012). An automated method for varve interpolation and its application to the Late Glacial  
968 chronology from Lake Suigetsu, Japan. *Quaternary Geochronology*, **13**, 52–69. doi:  
969 10.1016/j.quageo.2012.07.005

970 Scholaut, G., Brauer, A., Nakagawa, T., Lamb, H. F., Tyler, J. J., Staff, R. A., Marshall, M. H., Bronk  
971 Ramsey, C., Bryant, C. L., and Tarasov, P. E. (2017). Evidence for a bi-partition of the Younger  
972 Dryas Stadial in East Asia associated with inversed climate characteristics compared to  
973 Europe. *Scientific Reports*, **7**, 44983. doi: 10.1038/srep44983

974 Scholaut, G., Staff, R. A., Brauer, A., Lamb, H. F., Marshall, M. H., Bronk Ramsey, C., and Nakagawa,  
975 T. (2018). An extended and revised Lake Suigetsu varve chronology from ~50 to ~10 ka BP  
976 based on detailed sediment micro-facies analyses. *Quaternary Science Reviews*, **200**, 351–  
977 366. doi: 10.1016/j.quascirev.2018.09.021

978 Shigematsu, T., Tabushi, M., Nishikawa, Y., Muroga, T., and Matsunaga, Y. (1961). Geochemical  
979 Study on Lakes Mikata. *Bulletin of the Institute for Chemical Research, Kyoto University*, **39**(1),  
980 43-56.

981 Smith, V. C., Mark, D. F., Staff, R. A., Blockley, S. P., Bronk Ramsey, C., Bryant, C. L., Nakagawa, T.,  
982 Han, K. K., Weh, A., Takemura, K., and Danhara, T. (2011). Toward establishing precise  
983  $^{40}\text{Ar}/^{39}\text{Ar}$  chronologies for Late Pleistocene palaeoclimate archives: An example from the  
984 Lake Suigetsu (Japan) sedimentary record. *Quaternary Science Reviews*, **30**(21-22), 2845–  
985 2850. doi: 10.1016/j.quascirev.2011.06.020

986 Sone, T., Kano, A., Okumura, T., Kashiwagi, K., Hori, M., Jiang, X., and Shen, C. C. (2013). Holocene  
987 stalagmite oxygen isotopic record from the Japan Sea side of the Japanese Islands, as a new  
988 proxy of the East Asian winter monsoon. *Quaternary Science Reviews*, **75**, 150–160. doi:  
989 10.1016/j.quascirev.2013.06.019

990 Staff, R. A., Ramsey, C. B., Bryant, C. L., Brock, F., Payne, R. L., Scholaut, G., Marshall, M. H., Brauer,  
991 A., Lamb, H. F., Tarasov, P. E., Yokoyama, Y., Haraguchi, T., Gotanda, K., Yonenobu, H., and

- 992 Nakagawa, T. (2011). New <sup>14</sup>C determinations from Lake Suigetsu, Japan: 12,000 to 0 cal BP.  
993 *Radiocarbon*, **53**(3), 511–528. doi: 10.1017/S0033822200034627
- 994 Stein, A.F., Draxler, R.R., Rolph, G.D., Stunder, B.J.B., Cohen, M.D. and Ngan, F. (2015). NOAA’s  
995 HYSPLIT atmospheric transport and dispersion modeling system. *Bulletin of the American*  
996 *Meteorological Society*, **96**(12), 2059–2077. doi: 10.1175/BAMS-D-14-00110.1
- 997 Taniguchi, M., Nakayama, T., Tase, N., and Shimada, J. (2000). Stable isotope studies of precipitation  
998 and river water in the Lake Biwa basin, Japan. *Hydrological Processes*, **14**(3), 539–556. doi:  
999 10.1002/(SICI)1099-1085(20000228)14:3<539::AID-HYP953>3.0.CO;2-L
- 1000 Uemura, R., Yonezawa, N., Yoshimura, K., Asami, R., Kadena, H., Yamada, K., and Yoshida, N. (2012).  
1001 Factors controlling isotopic composition of precipitation on Okinawa Island, Japan:  
1002 Implications for paleoclimate reconstruction in the East Asian Monsoon region. *Journal of*  
1003 *Hydrology*, **475**, 314–322. doi: 10.1016/j.jhydrol.2012.10.014
- 1004 Vystavna, Y., Harjung, A., Monteiro, L.R., Matiatos, I., Wassenaar, L.I., 2021. Stable isotopes in global  
1005 lakes integrate catchment and climatic controls on evaporation. *Nature Communications*, **12**,  
1006 1–7. doi: 10.1038/s41467-021-27569-x
- 1007 Walker, M. J., Johnsen, S. J., Rasmussen, S. O., Popp, T., Steffensen, J.-P., Gibbard, P., Hoek, W. Z.,  
1008 Lowe, J., Andrews, J., Bjo, S., Cwynar, L. C., Hughen, K. A., Kershaw, P., Kromer, B., Litt, T.,  
1009 Lowe, D. J., Nakagawa, T., Newnham, R., Schwander, J., and Rck, B. (2009). Formal definition  
1010 and dating of the GSSP (Global Stratotype Section and Point) for the base of the Holocene  
1011 using the Greenland NGRIP ice core, and selected auxiliary records. *Journal of Quaternary*  
1012 *Science*, **24**(1), 3–17. doi: 10.1002/jqs.1227
- 1013 Wassenaar, L. I., Athanasopoulos, P., and Hendry, M. J. (2011). Isotope hydrology of precipitation,  
1014 surface and ground waters in the Okanagan Valley, British Columbia, Canada. *Journal of*  
1015 *Hydrology*, **411**(1–2), 37–48. doi: 10.1016/j.jhydrol.2011.09.032

- 1016 Xia, C., Liu, G., Hu, Y., and Meng, Y. (2018). Precipitation Stable Isotope Variability in Tropical  
1017 Monsoon Climatic Zone of Asia. *IOP Conference Series: Materials Science and Engineering*,  
1018 **392**(4). doi: 10.1088/1757-899X/392/4/042028
- 1019 Xia, Z., Welker, J.M. and Winnick, M.J. (2022). The Seasonality of Deuterium Excess in Non-Polar  
1020 Precipitation. *Global Biogeochemical Cycles*, **36**(10), e2021GB007245.  
1021 doi:10.1029/2021GB007245
- 1022 Xu, H., Goldsmith, Y., Lan, J., Tan, L., Wang, X., Zhou, X., Cheng, J., Lang, Y. and Liu, C. (2020).  
1023 Juxtaposition of Western Pacific Subtropical High on Asian Summer Monsoon Shapes  
1024 Subtropical East Asian Precipitation. *Geophysical Research Letters*, **47**(3), e2019GL084705.  
1025 doi: 10.1029/2019GL084705
- 1026